INSTITUTE OF PHYSICS PUBLISHING INVERSE PROBLEMS

Inverse Problems **18** (2002) R1–R28 PII: S0266-5611(02)24835-2

TOPICAL REVIEW

Mathematical problems in radar inverse scattering

Brett Borden

Research Department, Naval Air Warfare Center Weapons Division, China Lake, CA 93555-6100, USA

Received 8 October 2001
Published 19 December 2001
Online at stacks.iop.org/IP/18/R1

Abstract

The problem of all-weather noncooperative target recognition is of considerable interest to both defense and civil aviation agencies. Furthermore, the discipline of radar inverse scattering spans a set of real-world problems whose complexity can be as simple as perfectly conducting objects in uniform, isotropic, and clutter-free environments but also includes problems that are progressively more difficult. Consequently, this topic is attractive as a practical starting point for general object characterization schemes. But traditional radar target models—upon which most current radar systems are based—are nearing the end of their usefulness. Unfortunately, most traditional research programmes have emphasized instrumentation over image and model analysis and, consequently, the discipline is unnecessarily jargon-laden and device-specific. The result is that recent contributions in advanced imaging, inverse scattering and model fitting methods have often been 'excluded' from mainstream radar efforts. This topical review is intended to serve as a survey of current and proposed schemes and an overview and discussion of roadblocks to successful implementation of some of the more popular approaches. The presentation has been constructed in a manner that (it is hoped) will appeal to those physicists and applied mathematicians who are not approaching the subject of radar imaging from a formal radar background.

1. Introduction

Sensor systems that can detect and locate objects at great distances and in all kinds of weather have special utility and it has long been recognized that such systems can be created using active radio frequency (RF) electromagnetic transmitters and receivers. The first echo-location devices of this kind date to the early years of the 20th century and are favoured over traditional optical systems because the lower frequencies of RF waveforms render them relatively unattenuated by smoke, clouds, dust and precipitation.

When it comes to *imaging*, however, RAdio Detection And Ranging (radar) systems suffer in comparison with their optical counterparts—the lower frequency of RF waveforms also means that radar-based images of distant objects will generally fail to meet optical resolution standards. Consequently, RF and optical systems are often considered to be complementary

and disjoint: radar components are relegated to detection and location tasks; image formation is held to be an optics issue. All-weather long-range imaging problems have not been embraced by either camp.

1.1. Methods for all-weather object identification

Usually 'image formation' is not always required for object identification, of course, and sensor scientists have devised a variety of RF-appropriate methods for classifying and recognizing distant objects. The most common and, in principle, the simplest of these schemes uses a transponder mounted on the object itself to broadcast a (sometimes encoded) description of its identity. Another popular approach uses the fact that flying objects typically have oscillatory structural components (propellers, engine turbine blades, etc) that will modulate the reflected waveform in a uniquely characteristic way [7, 24, 72].

Other ideas have been proposed: polarization-based classifiers rely on the vector nature of electromagnetic fields and the fact that objects will depolarize a scattered waveform in a distinctive fashion [18, 19, 33, 40, 44, 61, 69, 75]. Radar-interrogated objects can also be treated as analogous to 'ringing bells'—an incident electromagnetic pulse may excite radiating body resonances that are determined by the object's size and shape [5, 6, 13, 25, 39, 71, 79, 90, 91, 104, 105, 114, 145]. Such depolarization, resonance, and/or modulation effects can be observed and compared to a library of known 'signatures' in order to classify or identify the illuminated body.

Unfortunately, these approaches all have their limitations—especially in environments where noise contamination may be significant and accurate object identification from arbitrary directions is essential. For these situations, true radar-based imaging strategies have been sought [2, 3, 8, 18, 20–24, 54, 66, 80, 83, 87, 93, 96, 97, 122, 125, 131, 134, 136, 137, 153, 154]. Radar image formation methods are (largely) based on inverse scattering concepts and, in this context, these methods are the subject of this topical review.

1.2. Paper overview

We assume that the reader has no prior radar knowledge and start out with a discussion of radar basics: signal representation, radar measurables and data acquisition. Such an opening naturally leads to a short description of electromagnetic scattering of radar waveforms and in section 3 we explain some of the standard approximations that lead to the weak, scattering-centre-based model.

Section 4 uses this scattering model to develop the radar imaging equation and examines the important issues of resolution and estimation error. The practical restrictions of this imaging equation to one and two dimensions (HRR and SAR, respectively) are explained in section 5. Section 6 discusses some of the principal implementation issues with these imaging schemes, as well as how radar images are used for object identification.

The last four sections are concerned with current research issues. Sections 7 and 8 explain how the standard weak scatterer model leads to image reconstruction artefacts and how these artefacts might be mitigated. Section 9 offers an overview of superresolution methods. And section 10 concludes with a brief discussion of other radar imaging problems and future research and development trends.

2. Radar basics

Radar systems have evolved over the past seven decades to efficiently perform a variety of very complex functions. Foremost among such functions are those associated with detecting

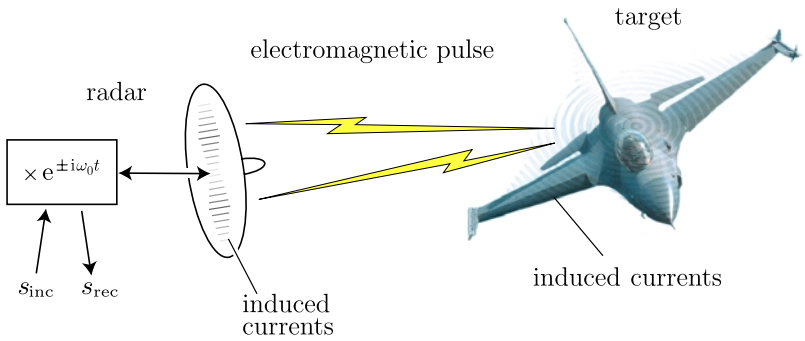

Figure 1. A generic radar detection system.

and locating radar *targets*[1]. Active radar systems accomplish these tasks by transmitting an electromagnetic waveform and measuring the reflected field as a time-varying voltage in the radar receiver. If R denotes the distance from the transmitter to the target, then the radiation condition guarantees that the energy in the transmitted field will decay as R^{-2} when R is sufficiently large (this is the usual case). The energy reflected by the target will also obey this radiation condition and so, in *monostatic* radar configurations (in which the radar transmitter and receiver are co-located), the energy collected by the receiver will be reduced from that transmitted by a factor of R^{-4}. In practice, this received energy is quite small, and when the target is far away the measured signal competes for attention with the thermal noise voltage of the radar system itself. Accurately separating the wanted signal from the unwanted noise is an impressive engineering feat and it is not surprising that a fair amount of device-specific jargon has evolved over the years. This section will briefly explain the methods employed.

Figure 1 shows the main elements of a generic (and greatly simplified) radar measurement system (cf [11, 82, 96, 127], and references cited therein). An incident time-varying signal $s_{\text{inc}}(t)$ is mixed with a *carrier signal* with (angular) frequency ω_0 chosen to conform with favourable properties of the transmission medium (typically, *atmospheric windows* are sought for which free space parameters are good approximations). This mixed signal is used to excite currents on an antenna that cause an electromagnetic waveform to be launched toward the target. (This antenna is rarely an isotropic radiator: it is usually designed to have some degree of directionality (*gain*), and this directionality can also be used to estimate target *bearing*.) The waveform is reflected from the target and the reciprocal situation occurs in the receiver: the reflected field induces antenna currents; the signal voltage is mixed with a conjugate carrier to remove (*beat down*) the carrier frequency dependence; and the time-varying voltage $s_{\text{rec}}(t)$ is output to a signal processor. Note that, while high frequencies dominate the target scattering physics (ω_0 is typically 1–35 GHz), the signal processing block usually sees much lower frequencies ($\omega \lesssim 0.1\omega_0$).

2.1. I and Q signals

The system signals are real-valued voltages and are often expressed in terms of circular functions $p(t) = a(t)\cos\phi(t)$ so that the concepts of amplitude and phase may be introduced. It is convenient, however, to consider the signals to be complex-valued, with $s(t) = \frac{1}{2}(p(t) + iq(t))$ for some $q(t)$. Of course, the choice of $q(t)$ is not unique and,

[1] A radar *target* is any object of interest illuminated by the radar. In contrast, radar *clutter* is composed of collateral and undesired illuminated objects.

moreover, this choice will affect the definition of the signal phase. The *quadrature phase* convention requires $s(t)$ to be analytic on the half-plane so that $p(t)$ and $q(t)$ are Hilbert transform pairs:

$$q(t) = \mathcal{H}\{p\}(t) = \frac{1}{\pi} \int_{\mathbb{R}} \frac{p(t')}{t - t'} \, \mathrm{d}t'. \tag{1}$$

The Hilbert transform can be expressed in terms of the Fourier transform $\mathcal{F}\{\cdot\}$ as[2] $\mathcal{H}\{p\}(t) = -\mathrm{i}\mathcal{F}^{-1}\{\mathrm{sgn}(\omega)\mathcal{F}\{p\}(\omega)\}(t)$. In practice, the range of values of ω is small enough that equation (1) can be estimated using the *narrowband approximation* [110] for which $\mathcal{H}\{a(t)\cos\phi(t)\}(t) \approx a(t)\sin\phi(t)$. Conveniently, this approximation can be implemented in hardware—if $p_{\mathrm{rec}}(t) = a(t)\cos(\phi(t) + \omega_0 t)$ is the (real-valued) voltage output from the receiving antenna, then the *in-phase* and *quadrature* components of $s_{\mathrm{rec}}(t)$ are found by mixing, phase shifting and low-pass filtering ($\mathrm{F_{LP}}\{\cdot\}$):

$$\begin{aligned} I(t) &= \mathrm{F_{LP}}\{p_{\mathrm{rec}}(t) \times \cos(\omega_0 t)\} = \tfrac{1}{2} a(t)\cos\phi(t) \\ Q(t) &= \mathrm{F_{LP}}\left\{\exp\left(\mathrm{i}\frac{\pi}{2}\right) p_{\mathrm{rec}}(t) \times \cos(\omega_0 t)\right\} = \frac{1}{2} a(t)\sin\phi(t). \end{aligned} \tag{2}$$

Because of this result, we can write arbitrary radar signals in the form $s_{\mathrm{rec}}(t) = a(t)\,\mathrm{e}^{\mathrm{i}\phi(t)}$. The function $a(t)$ is known as the *envelope* and $\phi(t)$ is the *phase modulation*. For such signals we can define the *instantaneous frequency* [89] as $\omega_{\mathrm{inst}} = \mathrm{d}\phi(t)/\mathrm{d}t$.

2.2. Radar measurables

In addition to target bearing (which we shall not consider further), radar systems usually estimate target *range* and *range-rate* [28, 43]. Assume that the transmission medium is well-approximated by the free-space constitutive parameters so that the propagation speed of the electromagnetic waveform will be c, the velocity of light in a vacuum. If a pulse is transmitted and the corresponding reflected signal is received after a time t, then the range to the target can be estimated to be $R = ct/2$. (Naturally, the estimation accuracy will depend on the pulse's time duration and narrower time domain pulses usually allow for better range estimation accuracy.)

In a similar way, a narrow frequency domain pulse (i.e. one whose Fourier domain support has negligible width) can be used to estimate the Doppler frequency shift ν imparted to the reflected field by the moving target. If ω_0 denotes the frequency of this transmitted waveform, then the radial velocity of the target can be estimated as $v_R = -c\nu/2\omega_0$.

Because range and range-rate are linearly scaled time delay and frequency shift, respectively, it will be notationally convenient to refer to t as the 'range variable' and ν as the 'range-rate variable' (when this can be done without confusion). When these two parameters are the only ones measured by the radar, then the *isotropic point scatterer* target model allows us to express the radar signal associated with the field reflected from an object at range t and radial velocity ν as

$$s_{\mathrm{scatt}}(t') = \rho\, s_{\mathrm{inc}}(t' - t)\,\mathrm{e}^{\mathrm{i}\nu(t'-t)} \tag{3}$$

where ρ is a signal strength scale factor, to be discussed below.

2.3. Correlation reception

The original radar signal processing problems are those of optimal detection and estimation in (additive) noise so that the received signal is of the form $s_{\mathrm{rec}}(t) = s_{\mathrm{scatt}}(t) + n(t)$, where $n(t)$ is

[2] Note that this relationship implies that $\mathrm{supp}(\mathcal{F}\{s\}(\omega)) \subset \mathbb{R}_+$.

a random noise process with probability density $p_N(n)$. Estimation is typically accomplished using maximum likelihood methods that compare $s_{\rm rec}(t)$ to an idealized family of signals created using a signal model. We assume that this model is unique and that there is no *a priori* target information so that the statistical nature of $s_{\rm rec}(t)$ is due only to the random nature of $n(t)$. Then the maximum likelihood estimate for $s_{\rm scatt}(t)$ is obtained from

$$s_{\rm scatt}^{\rm (ML)} = \arg \max_{s \in \text{model space}} p_N(s_{\rm rec} - s). \tag{4}$$

It is usual to parametrize the model space to facilitate the search for $s_{\rm scatt}^{\rm (ML)}$. For an active radar system seeking to estimate range and range-rate, the natural parametrization is just that of the isotropic point scatterer. Radar receiver noise is well modelled by Gaussian white-noise statistics and, in this case, it follows from equations (3) and (4) that the maximum likelihood estimate of t and ν is

$$t, \nu = \arg \max_{t', \nu'} \operatorname{Re}\{\eta(t', \nu')\} \tag{5}$$

where

$$\eta(t, \nu) = \int_{\mathbb{R}} s_{\rm rec}(t')\, s_{\rm inc}^{*}(t' - t)\, \mathrm{e}^{-\mathrm{i}\nu(t'-t)}\, \mathrm{d}t'. \tag{6}$$

The quantity $\eta(t, \nu)$ is the data output from the radar *correlation receiver* and is the basis for our remaining discussion [43, 68, 124, 157]. Correlation reception compares the received signal with reference signals of the form (3). This comparison is performed *coherently*, meaning that the phase of the transmission signal is preserved in the reference signal. The correlation receiver is also sometimes referred to as the *matched filter* receiver and this parameter estimation scheme maximizes the signal-to-noise power ratio [109]. (It can be shown that correlation reception also results in optimal detection, in the sense of the Neyman–Pearson lemma.)

2.4. Radar cross section

For the canonical isotropic point scatterer considered so far, the signal strength scale factor ρ, introduced in equation (3), will be independent of t, ν and target orientation—this is the reason that equation (5) exhibits no ρ dependence. But when measurements from real radar targets are analysed, the signal strength displays decidedly *non*-isotropic point scatterer behaviour. The *radar cross section* (RCS) is a measure of the energy reflected from the target and is usually expressed as a function of target orientation.

The cross section is not a target imaging concept—rather, it is a target detection tool. And, unlike isotropic points, real-world target detectability can be dramatically affected by target orientation. Early radar systems often used low frequency waveforms and were primarily concerned with object discovery. These systems were designed to exploit the point scatterer model and the resulting accuracy was usually sufficient for non-imaging purposes. As frequency was increased (for improved resolution), however, the limitations of this model became increasingly obvious: a plot of target RCS can display wild variations with changing orientation. This property can be interpreted as a consequence of constructive and destructive interference of the field reflected from a *collection* of coherently illuminated point scatterers and it turns out that, while this simple idea does not tell the whole story, it nevertheless works pretty well.

3. The field scattered from a radar target

To understand why it is possible to (effectively) replace a radar target by an 'equivalent' collection of localized scatterers, we need to examine the high frequency behaviour of

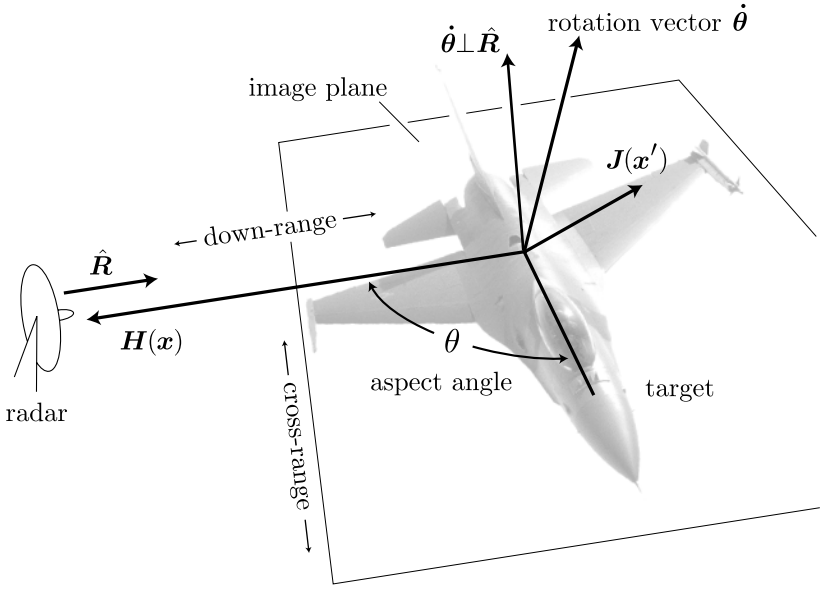

Figure 2. Scattering and imaging geometry.

electromagnetic scattering from geometrically complex bodies. We begin by examining an integral equation that is often used to determine the magnetic field scattered from a perfect conductor $D \subset \mathbb{R}^3$ in free space.

Physically, an electromagnetic wave $\boldsymbol{H}_{\text{inc}}(\boldsymbol{x}, t)$ incident upon D will excite currents $\boldsymbol{J}(\boldsymbol{x}', t')$ at time t' and position $\boldsymbol{x}'$ on the boundary ∂D of D. These currents will create a response field $\boldsymbol{H}_{\text{scatt}}(\boldsymbol{x}, t)$—the *scattered field*—which is to be measured and used to determine $\boldsymbol{J}$. Information about ∂D is encoded into $\boldsymbol{H}_{\text{scatt}}$ through $\boldsymbol{J}$. In general, $\boldsymbol{J}$ will not be restricted to ∂D and we must rely on some additional model if we are to estimate ∂D. Here, the perfect conductor assumption (no currents within D) is used because it is both tractable and applicable to traditional radar targets.

The basic scattering configuration is illustrated in figure 2. All coordinates are referenced to a point in the image plane (see section 5) fixed to a translating and rotating target. For reasons that will eventually become clear, it is convenient to choose this reference point to coincide with the instantaneous centre of rotation.

3.1. The magnetic field integral equation

Assume that the boundary of D is smooth everywhere and let $\hat{\boldsymbol{n}}$ denote the outwardly directed unit normal to ∂D at $\boldsymbol{x}'$. Straightforward application of Maxwell's equations, and applying the perfect conductor boundary condition, yields the induced-current space–time integral equation [106, 116, 132]

$$\boldsymbol{J}(\boldsymbol{x}', t') = 2\hat{\boldsymbol{n}} \times \boldsymbol{H}_{\text{inc}}(\boldsymbol{x}', t') + \hat{\boldsymbol{n}} \times \frac{1}{2\pi} \oint_{\partial D} \mathcal{L}_r\{\boldsymbol{J}\}(\boldsymbol{x}'', t'') \times \hat{\boldsymbol{r}} \, \mathrm{d}S'' \tag{7}$$

where $\boldsymbol{r} = \boldsymbol{x}' - \boldsymbol{x}''$, $r = |\boldsymbol{r}|$, $\hat{\boldsymbol{r}} = \boldsymbol{r}/r$, $t'' = t' - r/c$ is the retarded time and $\mathcal{L}_r\{\boldsymbol{J}\}(\boldsymbol{x}'', t'') \equiv \left(r^{-2} + (rc)^{-1}\partial/\partial t''\right) \boldsymbol{J}(\boldsymbol{x}'', t'')$.

Equation (7) is a second-kind equation and, in principle, can be solved for $\boldsymbol{J}(\boldsymbol{x}', t')$. The scattered field can be expressed in terms of this surface current by

$$\boldsymbol{H}_{\text{scatt}}(\boldsymbol{x}, t) = \frac{1}{4\pi} \int_{\partial D} \mathcal{L}_R\{\boldsymbol{J}\}(\boldsymbol{x}', t') \times \hat{\boldsymbol{R}}\, \mathrm{d}S' \tag{8}$$

where $\boldsymbol{R} = \boldsymbol{x} - \boldsymbol{x}'$.

Multiple scattering events are accounted for by the integral term in equation (7). When the total contribution to $\boldsymbol{J}$ due to these subsequent field interactions is small in comparison to the initial driving field $2\hat{\boldsymbol{n}} \times \boldsymbol{H}_{\text{inc}}$ we can approximate

$$\boldsymbol{J}(\boldsymbol{x}', t') \approx \boldsymbol{J}_{\text{po}}(\boldsymbol{x}', t') = \begin{cases} 2\hat{\boldsymbol{n}} \times \boldsymbol{H}_{\text{inc}}(\boldsymbol{x}', t') & \text{if} \quad \hat{\boldsymbol{R}} \cdot \hat{\boldsymbol{n}} < 0 \\ 0 & \text{otherwise.} \end{cases} \tag{9}$$

This is the *physical optics* (or 'weak scatterer') approximation. The physical optics field scattered by D is defined from equation (8) by

$$\begin{aligned} \boldsymbol{H}_{\text{po}}(\boldsymbol{x}, t) &\equiv \frac{1}{4\pi} \int_{\partial D} \mathcal{L}_R\{\boldsymbol{J}_{\text{po}}\}(\boldsymbol{x}', t') \times \hat{\boldsymbol{R}}\, \mathrm{d}S' \\ &= \frac{1}{2\pi Rc} \int_{\hat{\boldsymbol{R}} \cdot \hat{\boldsymbol{n}} < 0} \hat{\boldsymbol{R}} \cdot \hat{\boldsymbol{n}}\, \frac{\partial \boldsymbol{H}_{\text{inc}}(\boldsymbol{x}', t')}{\partial t'}\, \mathrm{d}S' + \mathrm{O}(R^{-2}) \end{aligned} \tag{10}$$

where the integral is restricted to the illuminated portion of ∂D and we have assumed that the target dimensions are small with respect to R so that the R^{-1} factor can be brought out from under the integral sign. The physical optics *far field* approximation, appropriate to radar problems, drops the $\mathrm{O}(R^{-2})$ terms.

In the frequency domain, the incident field will have components of the form $\boldsymbol{H}_{\text{inc}}(\boldsymbol{x}, t) = \boldsymbol{H}_0 \mathrm{e}^{\mathrm{i}(k\hat{\boldsymbol{R}} \cdot \boldsymbol{x} + kR - \omega t)}$, where $k = \omega/c$. Substitution yields

$$\boldsymbol{H}_{\text{po}}(\boldsymbol{x}, t; k) = -\frac{\mathrm{i}k\boldsymbol{H}_0 \mathrm{e}^{\mathrm{i}(2kR - \omega t)}}{2\pi R} \int_{\hat{\boldsymbol{R}} \cdot \hat{\boldsymbol{n}} < 0} \hat{\boldsymbol{R}} \cdot \hat{\boldsymbol{n}}\, \mathrm{e}^{\mathrm{i}2k\hat{\boldsymbol{R}} \cdot \boldsymbol{x}'}\, \mathrm{d}S'. \tag{11}$$

Since ∂D is smooth, we can evaluate equation (11) by the method of stationary phase [15, 16]. In the high frequency limit the first-order *geometric optics* approximation becomes [66, 74, 154]

$$\begin{aligned} \boldsymbol{H}_{\text{go};1}(\boldsymbol{x}, t; k) &\equiv \lim_{\text{large } k} \boldsymbol{H}_{\text{po}}(\boldsymbol{x}, t; k) \\ &= -\frac{\mathrm{i}k\boldsymbol{H}_0 \mathrm{e}^{\mathrm{i}(2kR - \omega t)}}{2\pi R} \sum_m A_m \mathrm{e}^{\mathrm{i}2k\hat{\boldsymbol{R}} \cdot \boldsymbol{x}_m} + \mathrm{O}(k^0) \end{aligned} \tag{12}$$

where the sum is over all points on ∂D at which $\hat{\boldsymbol{R}} \cdot \hat{\boldsymbol{n}} = -1$ and A_m denotes the contribution to the integral in (11) of the local neighbourhood $\mathcal{N}_{\boldsymbol{x}_m} \subset \partial D$ of $\boldsymbol{x}_m$.

3.2. Polarization

Significantly, equations (10) and (12) are depolarization insensitive—that is, the approximate scattered field is a simple scalar multiple of the incident field with the vector orientation unchanged. This same-sense polarization behaviour between $\boldsymbol{H}_0$ and $\boldsymbol{H}_{\text{scatt}}$ is generally unphysical and, in those cases where polarization-diverse measurements can be made, a more complete scattering model is needed.

For smooth ∂D the depolarization effects will evidently be determined by the multiple interaction integral of equation (7), and a first-order correction to the physical optics field has been achieved by expanding the space–time integral equation for a perfect conductor in a Neumann series and truncating after the second term [9, 19, 24]. In this way it can be shown that

the amount of depolarization induced by smooth convex targets is proportional to the difference in the local principal curvatures of ∂D. More complex target geometries, however, warrant a more complete analysis and an expedient approach to polarization modelling approximates the local scattered field by rigorous polarimetric solutions for canonical shapes [61]. In this way, the simple behaviour of the geometric optics approximation can be retained by replacing the product $\boldsymbol{H}_0 \cdot A_m$ in equation (12) with a complex-valued vector quantity $\boldsymbol{A}_{m;\boldsymbol{H}_0}$.

Given that most radar systems acquire data that are restricted to a single polarization, it is meaningful to try to assess the advantage gained for a particular application by including these additional full-vector effects. Polarization-diverse radar systems are generally much more complex than their scalar counterparts. Despite this drawback, it is often argued that the extra complications are worth the effort because of the additional target information available to identification schemes [18, 19, 33, 44]. In addition, since targets and clutter often depolarize the incident field in very different ways, polarization methods can be used for clutter rejection.

3.3. Some ad hoc modifications

When ∂D is not smooth, equations (7) and (8) require only minor modification, but when D is not perfectly conducting the induced current integral equation will generally be much more complicated [116]. Complex target geometries can cause high frequency weak scatterer analysis to become very messy, even in the perfectly conducting case, however, and force-fitting physical or geometrical optics results to real world targets is more of an art than a science.

To begin with, the requirement that $\boldsymbol{J}_{\text{po}}$ vanish in the target's shadow region is simply unphysical. One possible fix for this limitation is to include the multiple interaction integral of equation (7) for those $\boldsymbol{x} \in \partial D$, where $\hat{\boldsymbol{R}} \cdot \hat{\boldsymbol{n}} \geqslant 0$, but this turns out to be much less useful than enhancements based on rigorous analysis of standardized targets. The uniform theory of diffraction (UTD) [144] effectively reformulates physical optics by appropriately appending induced currents associated with canonical discontinuities. In contrast to UTD, the geometric theory of diffraction (GTD) [67, 77, 78, 81] appends rigorous field solutions for canonical shapes and can be thought of as a reformation of geometric optics.

Other heuristics apply: smooth structures can be treated by ray techniques (i.e. geometric optics); isolated target structural elements are not 'turned on' (and so, do not scatter) if their characteristic size is much smaller than the incident field's wavelength (this is a resonance effect); and large complex structures can be replaced by a group of separate substructures [123]. Imperfect conductors can be described using impedance boundary conditions, the net effects of which do not significantly change the image-relevant behaviour of physical and geometrical optics. Dielectric scatterers can be handled using *apparent currents* and volume integrals [106].

All of this leads to a conventional radar imaging model in which the target is considered to be made up of *scattering centres* that can be used to determine $\boldsymbol{H}_{\text{scatt}}$ by asymptotic methods. Multiple scattering is ignored at this level of approximation and so equation (3) can be generalized by writing

$$s_{\text{scatt}}(t) = \int_{\mathbb{R}^2} \rho(t', \nu')\, s_{\text{inc}}(t - t')\, \mathrm{e}^{\mathrm{i}\nu'(t-t')}\, \mathrm{d}t'\, \mathrm{d}\nu'. \tag{13}$$

The scale factor ρ, introduced in (3), is now the *target reflectivity function* $\rho(t, \nu) : \mathbb{R}^2 \to \mathbb{C}$ and is defined in such a way that $\rho(t, \nu)\, \mathrm{d}t\, \mathrm{d}\nu$ is proportional to the field reflected from the target at range between $ct/2$ and $c(t + \mathrm{d}t)/2$ with Doppler shift between ν and $\nu + \mathrm{d}\nu$. (The possibility of polarization dependence will be deferred to section 8.1.)

4. The radar imaging equation

In general, the reflectivity function actually depends upon $\boldsymbol{H}_{\text{inc}}$ since local scattering behaviour varies with incident field direction and frequency content. But when the ranges of values for θ and ω are sufficiently restricted, we can make a radar imaging approximation that neglects this dependence (more about this in sections 7 and 8).

Radar imaging is subject to the same considerations as parameter estimation and the arguments leading to equation (6) apply—but now the data collected from the correlation receiver will not generally be those appropriate to the single-point target model of equation (3). To understand just what it is that the correlation receiver 'sees' in the extended target case, we substitute the model of equation (13) into (6) to yield

$$\eta(t,\nu) = \int_{\mathbb{R}^2} \rho(t',\nu')\,\chi(t-t',\nu-\nu')\,\mathrm{e}^{\mathrm{i}(\nu+\nu')(t-t')/2}\mathrm{d}t'\,\mathrm{d}\nu' + \text{correlation noise term} \tag{14}$$

where

$$\chi(t,\nu) \equiv \int_{\mathbb{R}} s^*_{\text{inc}}(t'-\tfrac{1}{2}t)\,s_{\text{inc}}(t'+\tfrac{1}{2}t)\,\mathrm{e}^{-\mathrm{i}\nu t'}\mathrm{d}t'. \tag{15}$$

Equation (14) is an imaging equation [124, 152] in which $\rho(t,\nu)$ is the object function and the remaining factors in the integrand represent an imaging kernel (a point-spread function). Consequently, $\eta(t,\nu)$ is an estimate of $\rho(t,\nu)$ and we can write $\hat{\rho}(t,\nu) = \eta(t,\nu)$. The additional noise term will be small when the noise process is uncorrelated with the transmission signal but can become large when $s_{\text{rec}}(t)$ displays other than white–Gaussian statistical behaviour (as will happen, for example, when radar clutter is present).

$\chi(t,\nu)$ is known as the *radar ambiguity function* and the ideal imaging kernel would be given by $\chi(t,\nu) = \delta(t)\delta(\nu)$. We shall see below that this is not allowed since the nature of $\chi(t,\nu)$ is such that an interrogating signal $s_{\text{inc}}(t)$ that leads to fine resolution in the t direction will generally have course resolution in the ν direction, and vice versa. Consequently, there will usually be a trade-off decision between resolution in t and ν that must be made by the radar design engineer based on the ultimate purpose of the radar data. Radar imaging systems usually choose good range resolution over good cross-range resolution.

The radar ambiguity function has been much studied [28, 43, 65, 103, 124, 157] in connection with the *ambiguity problem*: determination of s_{inc} from its ambiguity[3]. We will not consider this interesting issue and will simply observe that realizable measurement systems will obtain finite and band-limited data and will be unable to generate true δ functions in the time domain. This situation has an idealization that considers incident radar signals of the (frequency-domain) form

$$S(\omega) = \mathcal{F}\{s\}(\omega) = \sqrt{\frac{2\pi}{\Delta\omega}}\,\text{rect}\left(\frac{\omega+\omega_0}{\Delta\omega}\right) \qquad \omega \in (\omega_1,\omega_2) \tag{16}$$

where $\Delta\omega = \omega_2 - \omega_1$, $\omega_0 = \frac{1}{2}(\omega_1+\omega_2)$ and $\text{rect}(x) = 1$ if $x \in (-\frac{1}{2},\frac{1}{2})$ and 0 otherwise. The $\chi(t,\nu)$ associated with this signal is

$$\chi(t,\nu) = \frac{\Delta\omega - |\nu|}{\Delta\omega}\,\mathrm{e}^{\mathrm{i}(\omega_0+\nu/2)t}\,\text{sinc}\left[\tfrac{1}{2}(\Delta\omega-|\nu|)t\right] \qquad |\nu| \leqslant \Delta\omega \tag{17}$$

where $\text{sinc}(x) = \sin x/x$. By increasing $\Delta\omega$, this kernel can be made to more closely approximate $\delta(t)$.

[3] For target parameter estimation, the important quantity is the imaging kernel. For system design, the signal is the thing. The ambiguity problem is complicated by the fact that radar engineers are usually preoccupied only with the absolute value of the ambiguity function and, in this case, the generalized ambiguity problem seeks *all possible* $s_{\text{inc}}(t)$ yielding the required $|\chi(t,\nu)|$.

4.1. Radar uncertainty

The *instantaneous power* [28, 41, 43] in a signal $s(t) = a(t)\,\mathrm{e}^{\mathrm{i}\phi(t)}$ is defined to be $|s(t)|^2$. We assume the signal energy is normalized (i.e. $\int_{\mathbb{R}} |s(t')|^2\,\mathrm{d}t' = 1$) and that the power decays as $\lim_{t\to\pm\infty} t\,|s(t)|^2 = 0$. Then the *pulsewidth* is defined by

$$\Delta t = \left(\int_{\mathbb{R}} (t' - \bar{t}\,)^2\,|s(t)|^2\,\mathrm{d}t' \right)^{1/2} \tag{18}$$

where $\bar{t} = \int_{\mathbb{R}} t'\,|s(t)|^2\,\mathrm{d}t'$.

Similarly, if $S(\omega) = \mathcal{F}\{s\}(\omega)$ denotes the Fourier transform of $s(t)$, then the *power spectrum* is $|S(\omega)|^2$ and the *bandwidth* is

$$\Delta\omega = \left(\frac{1}{\pi} \int_{\mathbb{R}_+} (\omega' - \overline{\omega})^2\,|S(\omega)|^2\,\mathrm{d}\omega' \right)^{1/2} = \left(\int_{\mathbb{R}} \left| \frac{\mathrm{d}s(t')}{\mathrm{d}t'} \right|^2 \mathrm{d}t' - \overline{\omega}^2 \right)^{1/2} \tag{19}$$

where $\overline{\omega} = \frac{1}{\pi} \int_{\mathbb{R}_+} \omega'\,|S(\omega)|^2\,\mathrm{d}\omega'$ and the second result follows from Fourier analysis of the differentiable functions. The *error coupling coefficient* can be determined using the instantaneous frequency and is defined by

$$\alpha = \int_{\mathbb{R}} (t' - \bar{t}\,) \left(\frac{\mathrm{d}\phi(t')}{\mathrm{d}t'} - \overline{\omega} \right) |s(t')|^2\,\mathrm{d}t' = -\mathrm{Im} \left\{ \int_{\mathbb{R}} t'\,s(t')\,\frac{\mathrm{d}s^*(t')}{\mathrm{d}t'}\,\mathrm{d}t' \right\} - \bar{t}\,\overline{\omega}. \tag{20}$$

But, by direct calculation, we can show that

$$\mathrm{Re} \left\{ \int_{\mathbb{R}} t'\,s(t')\,\frac{\mathrm{d}s^*(t')}{\mathrm{d}t'}\,\mathrm{d}t' \right\} = -\frac{1}{2}. \tag{21}$$

The Schwartz inequality, combined with the definitions (18)–(21), allows us to conclude that

$$[(\Delta t)^2 + \bar{t}^2][(\Delta\omega)^2 + \overline{\omega}^2] \geqslant \tfrac{1}{4} + (\alpha + \bar{t}\,\overline{\omega})^2. \tag{22}$$

This is the *radar uncertainty principle* and bounds the accuracy with which range and range-rate can be simultaneously estimated *using a single pulse*. (The 'usual' form of the uncertainty principle relies on a coordinate transformation to set $\bar{t} = \overline{\omega} = 0$. In this case, (22) becomes $(\Delta t\,\Delta\omega)^2 \geqslant \frac{1}{4} + \alpha^2$.)

4.2. Estimation error

From definition (15) it can be seen that $|\chi(0, 0)|$ is equivalent to the energy E of the radar pulse. If σ^2 denotes the noise energy, then $|\chi(0, 0)| - \sigma^2$ will represent the maximum energy 'usable' for target parameter estimation. Level cuts of $\chi(t, \nu)$ near $(t, \nu) = (0, 0)$ are approximately elliptical and the $E - \sigma^2$ level cut is called the *uncertainty ellipse*: its dimensions yield the RMS estimation error as

$$\delta t_{\mathrm{rms}} = \frac{1}{\Delta\omega} \frac{\sigma}{\sqrt{2E}} \qquad \text{and} \qquad \delta \nu_{\mathrm{rms}} = \frac{1}{\Delta t} \frac{\sigma}{\sqrt{2E}}. \tag{23}$$

(This result follows from a Taylor series expansion of $\chi(t, \nu)$ near the origin.)

Equation (23) shows that range resolution is inversely proportional to bandwidth. This important observation is the motivation for high range-resolution systems based on *ultra-wideband signals* (UWB) [108] for which $\Delta\omega \gtrsim 0.25\,\omega_0$. (Note that the narrowband approximation is not valid in this case and some of the preceding analysis—in particular, the definition of the ambiguity function—needs to be reworked when dealing with UWB waveforms [135].)

The first equation of (23) is also the basis for the important concept of *pulse compression*. From equation (19), it is easy to see that

$$(\Delta\omega)^2 = \int_{\mathbb{R}} \left| \frac{\mathrm{d}a(t')}{\mathrm{d}t'} \right|^2 \mathrm{d}t' + \int_{\mathbb{R}} \left| \frac{\mathrm{d}\phi(t')}{\mathrm{d}t'} \right|^2 \left| s(t') \right|^2 \mathrm{d}t' - \overline{\omega}^2. \tag{24}$$

Consequently, a *nonlinear* $\phi(t)$ will always increase the bandwidth in comparison with signals that are modulated in amplitude only. (Linear ϕ would simply change the value of $\overline{\omega}$.) When a signal is phase modulated by a nonlinear ϕ, the signal is said to be *pulse compressed*. This observation is of practical importance since it allows for the creation of fine range-resolution waveforms that are also of long duration—thereby increasing the amount of energy the radar can 'put on target' without having to increase the peak power of the radar's transmitter.

A common pulse compression choice by radar engineers is *linear frequency modulation* (LFM) for which $\phi(t) = \frac{1}{2}\gamma t^2$. When $a(t) = \mathrm{rect}(t)$, an LFM pulse is called a *chirp*.

5. Radar images

5.1. One-dimensional imaging

Image resolution is determined by the ambiguity function and the simplest kind of radar image is obtained by selecting $\chi(t, \nu) \sim \delta(t)$ so that equation (14) becomes

$$\eta(t, \nu) \sim \int_{\mathbb{R}} \rho(t, \nu')\, \mathrm{d}\nu' \tag{25}$$

(suppressing the additive noise term). An image formed in this way is called a *range profile* and, since equation (25) is actually independent of ν, range profiles are maps of ρ, coherently summed over cross-range dimensions and expressed as functions of the range [1, 2, 70, 93].

Of course, $\chi(t, \nu) = \delta(t)$ is an idealization appropriate to *high range-resolution* (HRR) imaging. Owing to equation (23), any actual HRR interrogating pulse will necessarily be of large bandwidth and such imaging systems are also sometimes referred to as *wideband (imaging) radars*. Figure 3 shows an example of the kind of one-dimensional images that can be created by HRR radar systems. The range profile is from a Boeing 727 jetliner, a top view of which is displayed beneath (with orientation at the time of measurement). These data were collected using a radar with parameters $\Delta\omega = 2\pi \times 500$ MHz and $\overline{\omega} = \omega_0 = 2\pi \times 9.25$ GHz [140]. An approximate mapping between some of the range profile peaks and target features is also presented (vertical lines).

The strength and location of the peaks in a range profile define a one-dimensional target signature that can be used to help identify the target. Unfortunately, target orientation is not generally estimable from a range profile and—in this case—target identification really requires matching the profile to a template defined by target type as well as target aspect (see section 6.1). In addition, range profiles offer no cross-range information about the target: measured dependence on ν' typically requires multiple pulses obtained from different target aspects (although other possibilities have been proposed [12, 50]).

5.2. Two-dimensional imaging

The radar uncertainty relation guarantees that a simple pulse that yields high range resolution cannot be used to obtain high cross-range resolution. Unlike uncertainty in quantum mechanics, however, radar interrogation does not generally alter the system being examined and follow-on pulses can measure whatever is wanted. *Pulse train* measurements exploit this freedom and use sequential HRR pulses to interrogate the target: each individual pulse is used to probe the

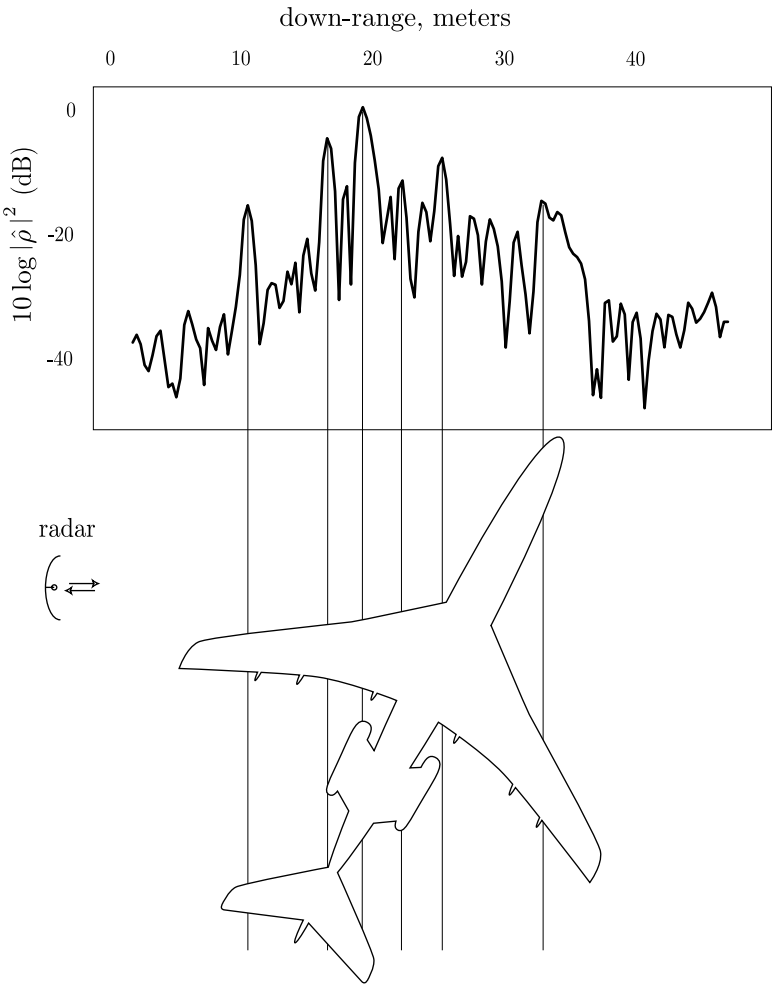

Figure 3. Example range profile of a Boeing 727 jetliner (top view positioned below the profile) created using a radar system with centre frequency 9.25 GHz and bandwidth 500 MHz.

target's range dimension while the overall pulse train duration is chosen large enough that (by equation (23)) good cross-range resolution can be achieved.

An equivalent—and somewhat more enlightening—interpretation of pulse train based imaging is made possible by introducing the notion of the *synthetic aperture.* Here, a family of signals $s_\theta(t)$, parametrized by target aspect θ, is used to build $\chi_\theta(t, \nu)$ that are independently localized along different target orientations. In (spotlight mode) *synthetic aperture radar* (SAR) imaging the target's aspect varies because of radar motion. In *inverse synthetic aperture radar* (ISAR), the aspect variation is due to target rotation. When the target can be assumed to rotate as a rigid body, then SAR and ISAR imaging are equivalent (except for geometry and clutter complications). The 'synthetic aperture' nature of the problem is a concept borrowed from optical imaging systems—large optical (and *real aperture radar* (RAR)) apertures generally yield finer resolution than small ones and the radar synthetic aperture is possible because the data are coherently collected over the range of aspects $\Delta\theta$ (the aperture) [26, 32, 34, 35, 48, 56–58, 64, 92, 93, 119, 120, 147, 155].

Assume, for simplicity, that the radar is configured to transmit a series of HRR pulses $s(t - jT)$, $j = 1, \ldots, \Theta$, with each pulse separated in time by the interval T. (T^{-1} is known as the *pulse repetition frequency* (PRF) and the need to correctly assign each received pulse to its corresponding transmitted pulse determines the *maximum unambiguous range* for the radar[4].) Assume also that the target rotates as a rigid body with constant rotation rate $\dot{\theta}$ and that the scattering components that make up the target are *persistent* (i.e. independent of θ over the aperture $\Delta\theta = (\Theta - 1)T\,\dot{\theta}$). Then the jth pulse will interrogate the rotated object function $\rho_\theta(t, \nu) = \rho(t\cos\theta_j + \alpha^{-1}\nu\sin\theta_j, -\alpha t\sin\theta_j + \nu\cos\theta_j)$, where $\theta_j = jT\,\dot{\theta}$ and $\alpha = \dot{\theta}\omega_0$ is a scale factor relating target dimensions in t to those in ν. Equation (14) becomes

$$\eta_{\theta_j}(t, \nu) = \int_{\mathbb{R}^2} \rho(t'\cos\theta_j + \alpha^{-1}\nu'\sin\theta_j, -\alpha t'\sin\theta_j + \nu'\cos\theta_j) \times \chi(t - t', \nu - \nu')\,\mathrm{e}^{\mathrm{i}(\nu+\nu')(t-t')/2}\,\mathrm{d}t'\,\mathrm{d}\nu'. \tag{26}$$

Substituting the HRR idealization $\chi(t, \nu) = \delta(t)$ yields the HRR range profile of the target at aspect θ_j:

$$\eta_{\theta_j}(t, \nu) = \int_{L(t;\theta_j)} \rho(t', \nu')\,\mathrm{d}l \tag{27}$$

where $\mathrm{d}l$ is the differential arc length along the line $L(t; \theta_j) = \{(t', \nu') \mid t'\cos\theta_j + \nu'\sin\theta_j = t\}$.

Equation (27) is the Radon transform of ρ and it is easy to see the relationship [46, 94, 95] between synthetic aperture imagery and tomographic reconstruction from this expression (recall that (27) is actually independent of ν). Two-dimensional estimates of ρ can be obtained from the data $\{\eta_{\theta_j} : j = 1, \ldots, \Theta\}$ by well-known inversion techniques—for example, by the *convolution-backprojection* algorithm [14, 107] —and the approach has been well studied in connection with medical imaging methods (but note that, in the present situation, $\eta_\theta(t, \nu) \in \mathbb{C}$).

The imaging configuration is illustrated in figure 2. The component of the target rotation vector $\dot{\boldsymbol{\theta}}$ perpendicular to $\boldsymbol{R}$ will define the normal to the image plane and ISAR images are projections of $\rho(t, \nu)$ onto this plane. The *down-range* and *cross-range* directions correspond to the t and ν coordinate axes, respectively. Figure 4 is an example ISAR image created from a Boeing 727 jetliner as it was taking off [140]. The target was located approximately three miles from the radar and was undergoing a steady turn while the radar measurements were made. The radar's centre frequency was $\overline{\omega} = \omega_0 = 2\pi \times 9.25$ GHz and its bandwidth was $\Delta\omega = 2\pi \times 500$ MHz. These data were collected over a short time (several seconds) and resulted in an overall aperture of $\Delta\theta \approx 2^\circ$.

6. Implementation issues

There are a variety of complications that conspire against the radar imaging practitioner, especially when the ultimate purpose of the radar images is target identification. Many of these problems are associated with the target model approximations that we have made so far: persistent and point-like scatterers; no multiple scattering effects; and target motion limited to rotations of constant rate. These issues will be examined in turn, but first we want to explain a simple and annoying consequence of the coherent nature of radar data.

6.1. Template-based HRR target identification

Target identification from radar images is usually accomplished by seeking the best fit between a measured image and one in a library $\mathcal{L}_N$ of known images [51, 60, 84, 128, 161]. The elements

[4] The product of PRF and Δt is the fraction of time that the radar is transmitting, or the *duty cycle*.

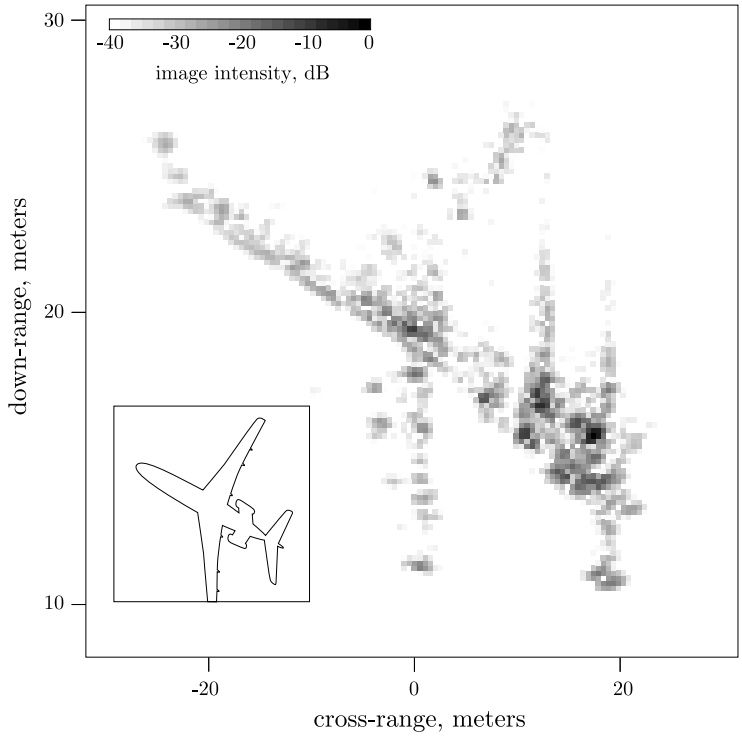

Figure 4. Example ISAR image. The image is the $|\rho(t, \nu)|^2$ of a Boeing 727 jetliner with orientation as in the inset. The radar centre frequency and bandwidth were 9.25 GHz and 500 MHz, respectively. Compare this figure with the range profile of figure 3.

of the library are called *templates*: $\tau_n \in \mathcal{L}_N$ where n indexes the N known targets in the library. In the case of range profile images the templates are functions of the range variable t and are parametrized by θ.

Let $\hat{\rho}(t)$ denote a range profile measured using an HRR radar. There are many ways to compare $\hat{\rho}(t)$ with $\tau_n(t; \theta)$, but one of the most common is based on the maximum correlation coefficient

$$C(n, \theta) = \max_{t \in \mathbb{R}} \int_{\mathbb{R}} \hat{\rho}(t')\, \tau_n(t' + t; \theta)\, \mathrm{d}t'. \tag{28}$$

Template correlation methods compute $C(n, \theta)$ for each $n = 1, \ldots, N$ and each $\theta = \theta_1, \ldots, \theta_M$. Target type and orientation are then estimated as

$$n, \theta = \arg \max_{\substack{n'=1,\ldots,N \\ \theta'=\theta_1,\ldots,\theta_M}} \left\{ C(n', \theta') \right\}. \tag{29}$$

The search over the M target orientations is required because it is impossible to divine target aspect from $\hat{\rho}(t)$ (and it must be implicitly understood that θ generally refers to an ordered pair of spherical angles). Typical libraries are set up with $N \approx 25$ 'targets of interest'. But, as we shall see below, there is little freedom in the choice of M.

6.2. Scintillation

Target *scintillation*[5] is a consequence of constructive and destructive interference of unresolved scattering centres that are coherently illuminated. The effect is easy to understand through the simple two-scatterer example illustrated in figure 5.

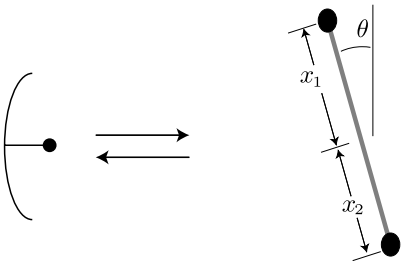

Figure 5. Scintillation example geometry.

If $k = \omega_0/c$ denotes the wavenumber of the incident field then the geometric optics scattered field will be

$$H_{\mathrm{go};1}(k,\theta) \sim a_1 \mathrm{e}^{\mathrm{i}2kx_1\theta} + a_2 \mathrm{e}^{\mathrm{i}2kx_2\theta} \tag{30}$$

where x_i denotes the scatterer cross-range coordinate evaluated at $\theta = 0$, a_i denotes scattering magnitude, and we have used the small angle approximation $\sin\theta \approx \theta$. In the simple case $a_1 \approx a_2$ it is easy to show that the scattered field energy varies with θ as

$$\left|\frac{H_{\mathrm{go};1}(k,\theta)}{H_{\mathrm{go};1}(k,0)}\right|^2 \approx \cos^2[k\theta(x_2 - x_1)]. \tag{31}$$

For typical radar frequencies ($\omega_0 \sim 2\pi \times 10$ GHz) and target sizes ($x_2 - x_1 \sim 10$ m) we have $k(x_2 - x_1) \gtrsim 100$. Scintillation effects, then, are observed as wild variations of radar cross section with small variations in θ and are expected to be common in radar data.

6.3. HRR and library searches

The effect of scintillation on HRR target identification can be understood from equation (31). Suppose our template matching scheme remains tolerant to peak variations in $\hat{\rho}(t)$ of up to 50%, but generally fails thereafter. Because of scintillation, the peaks can be expected to fluctuate by this amount for some angular variation $\delta\theta$. From (31) we have

$$\left|\frac{H_{\mathrm{go};1}(k,\delta\theta)}{H_{\mathrm{go};1}(k,0)}\right| = 0.5 \quad \Rightarrow \quad \delta\theta < \frac{\cos^{-1}(0.5)}{k(x_2 - x_1)}. \tag{32}$$

For $k(x_2 - x_1) \gtrsim 100$ we obtain $\delta\theta \lesssim 0.5^\circ$ and this result implies that we must create reference templates $\tau_n(t;\theta)$ on a $0.5^\circ \times 0.5^\circ$ lattice (if we are to guarantee good target identification performance). But such a library would contain approximately $N \times M \approx N \times 4\pi/(0.5\pi/180)^2 \sim N \times 10^6$ templates. This simple analysis reflects the situation observed in practice and, while the creation of such libraries is possible, searching through these libraries can be very time consuming since $C(n,\theta)$ must be calculated for all templates [128].

Various schemes have been proposed to make HRR template matching more amenable to real-time applications. These schemes generally rely on library thinning [115] (removing unlikely aspects or reducing lattice density at aspects for which $k(x_2 - x_1)$ decreases) and

[5] Note that the optics community usually applies the term 'scintillation' to atmospheric turbulence-induced transmission effects.

template feature minimization (only 'key' target features are stored in τ_n). Of course, computational engines are continually improving and this approach is expected to be part of target identification development programs for some time.

6.4. ISAR and motion compensation

The template library size problem is a consequence of the lack of target orientation information available from measured range profiles. It might be expected, then, that template matching with SAR/ISAR images will not suffer deleterious effects due to scintillation. Two-dimensional images *are* affected, however, and the main problem is a consequence of the fact that synthetic aperture images are generally constructed from range profiles.

The complicating issue is that target motion usually includes a translation component in addition to the required rotation. This translational motion must be carefully tracked and removed from subsequent range profiles before they can be transformed into the synthetic aperture image. The coherent nature of the radar data means that profile *range alignment* must be accurate to within a fraction of a wavelength $\lambda = 2\pi c/\omega_0$ (typically a few cm) since larger variations lead to significant phase errors that can adversely affect final image quality.

Range alignment is often accomplished with correlation methods that estimate corrective range offset by maximizing the correlation coefficient between time-translated succeeding profiles. When computation speed is required, sometimes only a few of the strongest peaks in the profiles are used to achieve 'bright spot' range alignment. Other methods are also used [17, 27, 29, 30, 32, 73, 86, 129, 146, 149, 151, 158, 159].

Target rotation rate and rotation axis are instantaneous notions and cannot be expected to apply to the target when the synthetic aperture $\Delta\theta$ is large (requiring long measurement intervals). Other target motions—such as roll, pitch and yaw, as well as target acceleration during measurement—can adversely affect simple range alignment methods and result in ISAR image blurring. The development of advanced motion compensation techniques that can deal with complex target motion is an active research area [36–38, 133, 134]. In practice, however, the problem is dealt with by simply restricting the data collection interval to a span in which $\dot{\boldsymbol{\theta}}$ can be considered constant.

6.5. Scintillation and motion compensation

Since range alignment is often just a correlation between subsequent range profiles, any sensitive variation that these profiles display as a function of aspect can be problematic. Scintillation, as unresolved subscatterer interference, manifests exactly this kind of sensitivity: both bright spot amplitude and position can fluctuate dramatically with changing θ. The net effect of scintillation on SAR/ ISAR imaging is an overall reduction in image quality.

Various solutions to this problem have been proposed and many of the most effective are based on other than correlation methods. For example, a polynomial fit to the target's range function $R(t)$ during the measurement interval can be used to provide a smooth estimate to the phase correction offset. These polynomials can be higher than first order in t since, in addition to range and range-rate, a series of Doppler measurements can be used to also estimate acceleration and jerk. Consequently, the phase correction can be found from

$$R(t) \approx R(0) + \dot{R}(0)t + \tfrac{1}{2}\ddot{R}(0)t^2 + \tfrac{1}{6}\dddot{R}(0)t^3. \tag{33}$$

(This method of motion compensation was used [141] to determine the pulse-to-pulse phase correction in figure 4.)

6.6. Principal limitations

While HRR images are easy to implement—they can be measured very quickly and require no sophisticated image formation algorithm—their utility is limited because they contain no target cross-range information. In addition, the lack of target orientation cues means that template matching libraries must contain profile-as-function-of-orientation data. And scintillation effects mandate that these libraries contain an unwieldy number of these templates, requiring lengthy computer searches if target identification is desired.

Synthetic aperture imaging is sometimes referred to as 'range-Doppler' imaging, although it is useful to recall that such images are actually based on tomographic principles. While cross-range and target orientation information is present, this information comes at the expense of significant computational time and complexity. The target's nonrotational motion components require careful accounting and, in practice, the inverse Radon transform is typically achieved using Fourier methods that require the data $\eta_\theta(t, \nu)$ (which are collected for (t, θ) on a polar grid) to be *polar reformatted* by interpolation to a rectangular grid [10, 76]. In addition, for ISAR image reconstruction the data are collected from a target rotating at an often unknown rate $\dot{\theta}$. Since the relative scaling between the down-range and cross-range target dimensions is proportional to $\dot{\theta}$, inaccurate estimates of the angular velocity can result in image scale distortion.

Unlike range profiles, two-dimensional radar imaging is difficult to implement and fine cross-range resolution requires long data collection intervals during which the radar remains trained on the target (long *dwell* times). Typically, however, the length of the data acquisition interval is limited to one in which $\dot{\boldsymbol{\theta}}$ can be considered to be constant, and this places an upper bound on the cross-range resolution in ISAR images of highly manoeuvering aircraft.

7. Image artefacts

Target recognition methods based upon one-or two-dimensional images can be severely stressed by the presence of image artefacts. Some of these artefacts can be understood in terms of the discussion so far—motion compensation errors, polar reformatting errors, scintillation 'noise'—and result in image degradation and localized blurring. Other image artefacts [24, 62] are consequences of fundamental limitations in the radar imaging equation and the point scatterer target model.

7.1. Isotropic points

The idealized concept of 'persistent, localized scattering centres' usually includes (implicitly) the notion that these scattering centres are well described by the geometric optics approximation. And, even though equation (12) is known to be inaccurate (recall the discussion of section 3.2), computational expediency is often invoked to justify the further simplification

$$\rho(t, \nu) = \sum_{n=1}^{N} a_n \, \delta(t - t_n)\delta(\nu - \nu_n). \tag{34}$$

Equation (34) is the *weak point scatterer model* and is routinely used in radar image reconstruction and analysis strategies. The low dimensionality of this model (three parameters per scattering centre) makes it very attractive for real-time applications and scattering centres are often argued to be 'effectively' point-like. Persistence of a_n with variable θ is clearly not a problem for range profiles and is also not usually an issue in two-dimensional images when $\Delta\theta$ is sufficiently restricted (as with ISAR imaging). The point-like nature of the model is a

more common limitation and misbehaved subscatterers include edges, gently curved plates and reentrant structures (ducts and cavities). In images, these features are underresolved, smudged, and sometimes physically displaced from the target elements that created them.

7.2. Structural dispersion

A medium is said to be dispersive if the waveform transmission speed depends on ω. *Structural dispersion* refers to geometrical shapes that display similar frequency dependence in transmission and scattering [31, 59, 63, 85, 100, 112, 113, 126, 148, 156]. The classic illustration of this effect is the simple parallel plate waveguide. Let k be the wavenumber along the transmission axis of the waveguide. The eigensolutions to the Helmholtz equation for this problem are called *modes* and the relationship between ω and k (the *dispersion relation*) can be shown to obey $\omega^2 = c^2(k^2 + \kappa_m^2)$, $m = 1, 2, \ldots$, where κ_m is a waveguide-dimension-dependent eigenvalue. The energy of these modal field solutions flows along the transmission axis with speed (group velocity)

$$v_m = \frac{\partial \omega}{\partial k} = \frac{c\,k}{\sqrt{k^2 + \kappa_m^2}}. \tag{35}$$

When $\omega < c\kappa_m$ the wavenumber will be imaginary and the wave will suffer exponential decay ($\omega_m = c\kappa_m$ is the mode *cutoff* frequency). Typically, $\kappa_m \propto m$ and so we can see that, as m increases, the radar pulse speed will decrease and scattering centres lying between the two plates will contribute terms to $\boldsymbol{H}_{\text{scatt}}$ that are time-delayed with respect to contributions from equirange scatterers that lie outside the waveguide.

Structural dispersion is associated with the ducts and cavities of a target. Consequently, the effects are common and can be observed at most target aspects. Unfortunately, the image components associated with dispersive scattering centres can be quite large in magnitude and, since they are displaced in range, can occlude other scattering centres. In extreme cases, the dispersive artefacts can be mistaken for target structures that do not really exist.

7.3. Multiple scattering

Another source of 'ghost artefacts' is illustrated by figure 6. Here, the weak scatterer approximation fails and secondary scattering has created a time-delayed image element that does not correspond to any weakly scattering structure.

Structural dispersion can be considered to be a type of multiple scattering event. Except for this limiting case, however, multiple scattering image ghosts are often weak and difficult to convincingly identify in actual images (although they are often invoked to explain measurement error). The notable exception to this trend is so-called *ground bounce* in which ground/target scattering interactions are often observed in SAR images of earth-bound buildings and vehicles.

8. Artefact mitigation

The weak point scatterer image model of equation (34) has proven to be quite useful in applications and radar image craftsmen have been loath to abandon it despite its recognized limitations. As far as target identification is concerned, image artefacts can be interpreted as additional image features and matched to templates that include these effects. Such feature-rich templates are very difficult to accurately create, however, and are unfeasible because of their sensitive dependence on minor target reconfiguration. This situation has fostered an

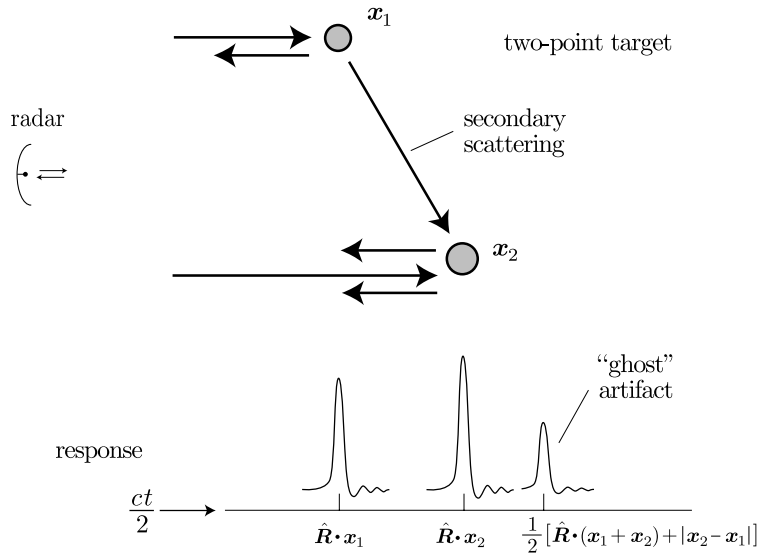

Figure 6. Illustration of multiple scattering induced image artefacts.

'artisanship' approach to image reconstruction and interpretation. Computation methods based on *expert system* strategies usually start from the viewpoint that the weak point scatterer model is 'mostly correct' and that experienced observers can tell the difference between scattering mechanisms by examining the radar image.

In practice, experienced observers *can* usually identify structural dispersion—although they often have less success with non-point-like and multiple scattering events. The goal of an expert system is to code this kind of intuition into computer software and apply the resulting algorithms as an aid to automatic target identification. 'Artificial intelligence' methods are often enlisted to help incorporate this sagacity and the field is an area of active research.

More traditional imaging methods (i.e. not expert system methods) are also being actively examined and, though less novel, usually have the advantage of more substantive analysis.

8.1. Point scatterer 'fixes'

The Fourier transform of the point scatterer model (34) yields

$$\begin{aligned}\mathcal{F}\{\rho(t,\nu)\}(\omega,\tau_\nu) &= \sum_{n=1}^{N}\mathcal{F}\{a_n\,\delta(t-t_n)\delta(\nu-\nu_n)\}(\omega,\tau_\nu)\\ &= \sum_{n=1}^{N} a_n\,\mathrm{e}^{-\mathrm{i}\omega t_n}\,\mathrm{e}^{-\mathrm{i}\tau_\nu \nu_n}\end{aligned} \tag{36}$$

and it is in this frequency domain that most model adjustment is performed.

Advanced parametric models replace a_n in the Fourier domain by $A_n(\omega,\theta)$ and apply localized scattering analysis to determine the ω and θ dependence [49, 53, 117, 118]. GTD calculations can be used to show that A_n has a frequency dependence obeying $A_n(\omega,\theta) \sim (\mathrm{i}\omega)^{\alpha_n}$, where $\alpha_n \in \{0, \pm\frac{1}{2}, \pm 1\}$ (corresponding to an important set of local target geometries). Similarly, the aspect dependence is approximated by $A_n(\omega,\theta) \sim \exp(\beta_n\theta)$, where β_n is a fitting parameter that accounts for amplitude variation with θ ($\beta_n = 0$ for an isotropic point). Possible polarization dependence is accommodated by replacing A_n with a vector-valued equivalent

$\boldsymbol{A}_n = [A_{11;n}, A_{12;n}, A_{22;n}]^T$: the components of this vector are complex valued (amplitude and phase) and A_{ij} denotes the j-polarized return from an i-polarized transmitted waveform.

In this way, the three-point model parameters $\{a_n, t_n, \nu_n\}$ are replaced with the extended parameter set $\{\alpha_n, \beta_n, \boldsymbol{A}_n, t_n, \nu_n\}$. The advanced parametric model can be written as

$$\mathcal{F}\{\boldsymbol{\rho}(t, \nu)\}(\omega, \tau_\nu) = \sum_{n=1}^{N} \boldsymbol{A}_n (\mathrm{i}\omega/\overline{\omega})^{\alpha_n} \mathrm{e}^{\beta_n \theta}\, \mathrm{e}^{-\mathrm{i}\omega t_n}\, \mathrm{e}^{-\mathrm{i}\tau_\nu \nu_n} \tag{37}$$

where the target reflectivity function now has a possible polarization dependence.

Other models attack the localized nature of the point scatterer model and replace the harmonic components $\mathrm{e}^{-\mathrm{i}\omega t_n}$ and $\mathrm{e}^{-\mathrm{i}\tau_\nu \nu_n}$ in equation (36) with modified undamped exponentials or damped exponential poles. These schemes can generally be related to the form of equation (37) and are sometimes useful in reducing its complexity for implementation simplicity.

For target identification and classification purposes, the advanced parametric models offer the possibility that local target structures can yield more clues to target identity than merely location and amplitude. But implementation of these ideas comes at a cost: accurate parameter extraction is computationally more complex than image formation and, more significantly, requires larger relative bandwidh and better signal-to-noise ratios [118].

8.2. Dispersive scatterer filtering

The waveguide dispersion relation shows that ω is a nonlinear function of k. In contrast, the field scattered from nondispersive scatterers obeys $\omega = ck$ and this difference has been the motivation for dispersion artefact filtering schemes [72, 98, 138, 139].

Time/frequency analysis [41] offers a means for determining a signal's frequency content as a function of time. In a t–ω plot, a time/frequency transform of the field scattered from an ordinary point scatterer will appear as a straight line $\delta(t - t_m)$ parallel to the frequency axis. Owing to the dispersion relation, however, the t–ω representation of a dispersive scatterer will be nonlinear. Consequently, it is possible to distinguish dispersive and nondispersive scattering mechanisms and, since inverse time/frequency transforms exist, pattern matching methods can be used to create dispersion artefact filtering techniques.

To date, these filtering methods have required either very large signal-to-noise ratios or very large signal bandwidths. Alternate methods are usually based on more complex model fitting approaches (i.e. more complete scattering models). More complex scattering models, of course, are also *more computationally expensive* scattering models—often, prohibitively so.

8.3. Multiple scattering enhancements

Perhaps the most difficult problems to address in a practical manner are those associated with multiple scattering ghosts. Typically, analysis starts with a naive model based on a one-dimensional target:

$$\eta(t) = \int_{\mathbb{R}} \rho(t')\, \chi(t - t')\, \mathrm{d}t' + \int_{\mathbb{R}^2} \rho(t')\, \rho(t'')\, \chi^{(2)}(t - t' - T_\rho(t', t''))\, \mathrm{d}t' \mathrm{d}t'' + \cdots. \tag{38}$$

Here, $\chi^{(2)}(t - t' - T_\rho(t', t''))$ is a suitably defined extension to the ambiguity function and $T_\rho(t', t'')$ is the time delay in signal transmission between $\rho(t'')$ and $\rho(t')$. In one dimension, $T_\rho(t', t'') = |t' - t''|$, but for real-world targets we are faced with a more complex model fitting situation in which three-dimensional targets must be justified against one-or two-dimensional image cues. Solution estimates are usually achieved by recursively fitting a parametrized version of the target to the data and can be impracticably computation-intensive (see also [150]).

More expedient methods are based on the observation that the single-scatter events that make up an ordinary radar image are connected to the target and obey rigid body motion in rotation. Multiple scattering artefacts will not obey such rigid body behaviour and the differences between radar images at different target aspects will identify the ghosts [143]. This approach requires at least two high resolution images from disparate target aspects and, though it enjoys intuitive appeal, it is difficult to apply in practice.

9. Image restoration and superresolution

'Superresolution' refers to any imaging method that improves the ability to distinguish two closely spaced image elements in comparison with the Nyquist resolution limit [130]. The importance of these methods extends beyond simple image contrast enrichment and scattering centre localization improvement—superresolution will also reduce scintillation effects associated with unresolved scatterers. Consequently, a large fraction of the radar imaging research effort has been spent in developing and improving resolution enhancing algorithms.

Roughly speaking, there are three categories into which superresolution methods are often grouped, although there is considerable overlap between the methods and this taxonomy can be somewhat misleading. Bandwidth extrapolation methods use the fact that $\mathcal{F}\{\rho\}(\omega, \tau_\nu)$ is analytic (this is guaranteed by the Polya–Plancherel theorem and the limited extent of $\mathrm{supp}(\rho(t, \nu))$). Consequently, Fourier domain data can, in principle, be determined everywhere from their measured values on a band-limited subset. Linear prediction models [55] are often used as the basis for this kind of analytic continuation, but methods invoking object support restriction (i.e. Landweber iteration or the Gerchberg–Papoulis algorithm) have also found favour [14, 52, 88, 121]. (Note, however, that while object support-constraint methods are applicable, other constraint-based schemes—such as object positivity, which is appropriate to optical imaging—cannot generally be used.)

The second general category of superresolution methods contains the parametric spectral estimation techniques [47, 102]. Of course, this subdivision includes most of the discussion of sections 4–8, starting with the maximum likelihood arguments used to motivate the radar imaging equation. Maximum likelihood strategies are not the only probabilistic methods used, however, and maximum *a posteriori* and maximum entropy [99, 130] schemes have also been proposed—especially when the additive measurement noise is known to be non-Gaussian. Model space refinement methods also often fall into this category: subspace fitting can be used to effectively separate the null space from the measurement space. This subspace partitioning may effectively reduce the dimensionality of the image reconstruction problem and ignore the noise components orthogonal to the model space.

Imaging kernels of the form of equation (17) are dominated by the $\mathrm{sinc}(\cdot)$ function which has a central peak (the *main lobe*) and damped oscillatory peaks (*side lobes*) on either side. In practice, most imaging kernels display this sinc dependence—the ambiguity function for a chirp obeys $\chi(t, \nu) \propto \mathrm{sinc}\,[\frac{1}{2}(\Delta t - |t|)(\nu - \gamma t)]$ where γ is the chirp rate—and the existence of side lobes is the most obvious difference between real imaging kernels and the idealized δ function kernel in affecting image resolution. Linear filtering schemes are often employed to reduce the effects of side lobes, but always at the expense of increased main-lobe width (and reduced resolution). The CLEAN algorithm [142] is a simple scheme that uses a parametric model of ρ (typically, the model of equation (34)), together with equation (14), to *iteratively* subtract the contribution of each scattering centre from the measured data. As a parametric model, CLEAN fits into the second category but, because the emphasis is on side-lobe reduction, it is often compared with the last superresolution group—the adaptive beamforming methods.

Adaptive beamforming is itself usually subdivided into those methods that are based on covariance matrix estimation schemes and those that are based on spatially variant filters. The first of these subgroups are probabilistic approaches that fit an idealized covariance matrix model to the measured radar data. Capon's minimum variance method [47] (a maximum likelihood approach) is of this form, as is the multiple signal classification (MUSIC) algorithm [111]. The second subdivision involves *nonlinear* filtering techniques to reduce side lobes while leaving the width of the main lobe unaffected. Space-variant filtering methods include adaptive side-lobe reduction (ASR) and the related special case of spatially variant apodization (SVA).

Ideally, of course, one would hope to develop waveforms with ambiguity functions that, if not a perfect $\delta(t)$, are at least perfect ridges in t–ν space (i.e. no side lobes). No single waveform can achieve this ideal autocorrelation but it is possible to find pairs of waveforms with the property that, if transmitted separately, the sum of the autocorrelations will have self-cancelling side lobes. Such *complementary pairs* are known but their practical utility is limited [103].

All superresolution methods apply *a priori* target information in one form or another and differing methods have varying sensitivity to this dependence. The extent to which resolution can be improved will always be directly related to the quality of the measured data. Analytic continuation, for example, is generally very sensitive to signal-to-noise ratio. But practical algorithmic implementation issues are often more important than stability since a too-slow algorithm yields no usable answer, even if it is robust against noise. The methods described above are often quite computationally intensive and there is no 'best approach' for all situations.

10. Conclusion

Our discussion has concentrated on ISAR and (spotlight) SAR and we have noted that the two imaging schemes are mathematically equivalent since they are related by a coordinate transformation. (The distinction all but vanishes for air-to-air imaging systems in which both target and radar are moving.) Other practical differences between SAR and ISAR, however, can be significant: SAR-based imaging must contend with ground clutter, target obscuration and antenna radiation anisotropy but is generally able to control radar/target relative motion; ISAR imaging is often unaffected by clutter and radiation pattern considerations but is severely restricted by unpredictable target maneuvers.

10.1. Other synthetic aperture imaging radar configurations

'Synthetic aperture radar' is an expression that also refers to other data collection configurations that we have not examined. *Stripmap* SAR is distinguished from spotlight SAR in that the radar antenna is fixed to—and points in a constant direction away from—a moving (usually aircraft) platform. Stripmap data are gathered from all targets that happen to be illuminated as a consequence of the radar's flightpath. Scan SAR is an intermediate configuration that uses independent antenna motion to collect data from directions other than those determined strictly by the flightpath, but are not restricted to spotlighting a specific target. Image reconstruction from data collected under these more general SAR configurations will obviously be different than in ISAR and spotlight SAR [56, 134].

Interferometric SAR (IFSAR and IFISAR) are radar modes that use multiple spatially offset data collection intervals in a scheme to create three-dimensional target reconstructions [4, 134, 160]. Akin to stereoscopic imaging, these methods suffer from all of the usual synthetic aperture target motion compensation issues plus the additional problems associated with 'data motion compensation' between the spatially disparate collection paths.

Ground penetrating radar [45, 101, 134] is a special class of increasingly important imaging problems that tax the practical capabilities of modern radar systems. Generally, soil and water are rather opaque at typical radar frequencies and objects buried more than about 10 cm deep are undetectable by radar signals with 10 GHz frequencies or higher. Low frequency radars ($\leqslant$500 MHz) are used to detect subsurface mines and unexploded ordinance, but these lower frequencies typically result in very coarse image resolutions. Moreover, subsurface clutter—in the form of soil dielectric anisotropy, stratification and rocks—present image interpretation issues that defy traditional radar analysis.

Finally, the concepts of bistatic and multistatic radar should be mentioned. Our review has considered only the 'simple' case of a co-located radar transmitter and receiver. In general, of course, this monostatic radar data collection configuration is not the only possible case and the possibility of separated transmitters and receivers is sometimes addressed. This situation includes the special situation where the transmitter is not traditional radar but, rather, may be broadcast radio (for example). In addition, since so-called 'stealthy' aircraft are usually designed with monostatic radars in mind, multi-static sensors may offer unique advantages.

10.2. Future trends and opportunities for applied mathematicians

Far from being a 'solved problem,' the discipline of radar imaging has yet to be fully developed. The weaknesses in the existing theory—particularly those associated with the weak scatterer approximation—mean that nonlinear effects are anticipated to be important in future radar image analysis efforts (these considerations are expected to be especially relevant to SAR-based imaging situations). A more complete scattering theory which includes multiple scattering terms will also need to address the practical issues of implementability in computationally limited real-time systems. Of course, efficient implementation issues in all aspects of radar-based image formation will continue to motivate research and development programmes.

But traditional image formation is intermediate to target identification and a number of important questions have gone unaddressed over the years. What, for example, is the totality of target-specific information contained in η and how can this information best be applied to the problem of target identification? HRR radar systems have been created with imaging criteria in mind, but reinterpretations of the radar imaging equation may well motivate new approaches to waveform design and efficient target parameter extraction.

Acknowledgments

This review is based on presentations given at the Mathematical Sciences Research Institute's Inverse Problems program in August of 2001. The author is grateful for the hospitality shown by the MSRI program organizers and the many useful subsequent discussions—especially those with Margaret Cheney and David Colton. This work was supported by the Office of Naval Research.

References

[1] Adachi S and Uno T 1993 One-dimensional target profiling by electromagnetic backscattering *J. Electromagn. Waves Appl.* **7** 403
[2] Ausherman D A, Kozma A, Walker J L, Jones H M and Poggio E C 1984 Developments in radar imaging *IEE Trans. Aerosp. Electron. Syst.* **20** 363
[3] Baltes H P (ed) 1980 *Inverse Scattering Problems in Optics, Topics in Current Physics* (New York: Springer)
[4] Bamler R and Hartl P 1998 Synthetic aperture radar interferometry *Inverse Problems* **14** R1

[5] Baum C E 1976 The singularity expansion method *Transient Electromagnetic Fields* ed L B Felsen (New York: Springer) p 130
[6] Baum C E, Rothwell E J, Chen K-M and Nyquist D P 1991 The singularity expansion method and its application to target identification *IEEE Proc.* **79** 1481
[7] Bell M R and Grubbs R A 1993 JEM modeling and measurement for radar target identification *IEE Trans. Aerosp. Electron. Syst.* **29** 73
[8] Bennett C L 1981 Time domain inverse scattering *IEEE Trans. Antennas Propag.* **29** 213
[9] Bennett C L, Auckenthaler A M, Smith R S and DeLorenzo J D 1973 Space time integral equation approach to the large body scattering problem *RADC-CR-73-70, AD763794* Sperry Rand Research Center, Sudbury, MA
[10] Berizzi F and Corsini G 1996 Autofocusing of inverse synthetic aperture radar images using contrast optimization *IEEE Trans. Aerosp. Electron. Syst.* **32** 1185
[11] Berkowitz R S *Modern Radar* (New York: Wiley)
[12] Bernfeld M 1984 Chirp Doppler radar *Proc. IEEE Lett.* **72** 540
[13] Berni A J 1975 Target identification by natural resonance estimation *IEEE Trans. Aerosp. Electron. Syst.* **11** 147
[14] Bertero M and Boccacci P 1998 *Introduction to Inverse Problems in Imaging* (Bristol: Institute of Physics Publishing)
[15] Bleistein N and Handelsman R A 1975 *Asymptotic Expansions of Integrals* (New York: Holt, Rinehart and Winston)
[16] Bleistein N 1989 Large wave number aperture-limited Fourier inversion and inverse scattering *Wave Motion* **11** 113
[17] Bocker R P and Jones S 1992 ISAR motion compensation using the burst derivative measure as a focal quality indicator *Int. J. Imaging Syst. Technol.* **4** 286
[18] Boerner W-M *et al* (ed) 1985 *Inverse Methods in Electromagnetic Imaging (NATO ASI Series, Series C: Mathematical and Physical Sciences vol 143)* (Dordrecht: Reidel)
[19] Boerner W-M 1980 Polarization utilization in electromagnetic inverse scattering *Inverse Scattering Problems in Optics* ed H P Baltes (New York: Springer) ch 7
[20] Bojarski N N 1967 Three-dimensional electromagnetic short pulse inverse scattering *Special Projects Lab. Report* Syracuse Univ. Res. Corp., Syracuse, NY
[21] Bojarski N N 1982 A survey of the physical optics inverse scattering identity *IEEE Trans. Antennas Propag.* **30** 980
[22] Borden B 1994 Problems in airborne radar target recognition *Inverse Problems* **10** 1009
[23] Borden B 1997 Some issues in inverse synthetic aperture radar image reconstruction *Inverse Problems* **13** 571
[24] Borden B 1999 *Radar Imaging of Airborne Targets: A Primer for Applied Mathematicians and Physicists* (Philadelphia, PA: Institute of Physics Publishing)
[25] Brittingham J N, Miller E K and Willows J L 1980 Pole extraction from real frequency information *IEEE Proc.* **68** 263
[26] Brown W M and Porcello L J 1969 An introduction to synthetic aperture radar *IEEE Spectrum* **6** 52
[27] Brown W M and Fredricks R J 1969 Range-Doppler imaging with motion through resolution cells *IEEE Trans. Aerosp. Electron. Syst.* **5** 98
[28] Burdic W S 1968 *Radar Signal Analysis* (Englewood Cliffs, NJ: Prentice-Hall)
[29] Cafforio C, Prati C and Rocca E 1991 SAR data focusing using seismic migration techniques *IEEE Trans. Aerosp. Electron. Syst.* **27** 194
[30] Calloway T M and Donohoe G W 1994 Subaperture autofocus for synthetic aperture radar *IEEE Trans. Aerosp. Electron. Syst.* **30** 617
[31] Carin L, Felsen L B, Kralj D, Pillai S U and Lee W C 1994 Dispersive modes in the time domain: analysis and time-frequency representation *IEEE Microw. Guid. Wave Lett.* **4** 23
[32] Carrara W G, Goodman R S and Majewski R M 1995 *Spotlight Synthetic Aperture Radar—Signal Processing Algorithms* (Boston, MA: Artech House Publishers)
[33] Chamberlain N F, Walton E K and Garber F D 1991 Radar target identification of aircraft using polarization-diverse features *IEEE Trans. Aerosp. Electron. Syst.* **27** 58
[34] Chen C-C and Andrews H C 1980 Multifrequency imaging of radar turntable data *IEEE Trans. Aerosp. Electron. Syst.* **16** 15
[35] Chen C-C and Andrews H C 1980 Target-motion-induced radar imaging *IEEE Trans. Aerosp. Electron. Syst.* **16** 2
[36] Chen V C and Qian S 1998 Joint time-frequency transform for radar range-Doppler imaging *IEEE Trans. Aerosp. Electron. Syst.* **34** 486

[37] Chen V C and Miceli W J 1998 Time-varying spectral analysis for radar imaging of maneuvering targets *IEE Proc., Radar Sonar Navig.* **145** 262
[38] Chen V C and Miceli W J 1999 Effect of roll, pitch and yaw motions on ISAR imaging *SPIE Proc. Radar Process. Technol. Appl.* **3810** 149
[39] Chuang C W and Moffatt D L 1976 Natural resonance of radar target via Prony's method and target discrimination *IEEE Trans. Aerosp. Electron. Syst.* **12** 583
[40] Cloude S R and Pottier E 1996 A review of target decomposition theorems in radar polarimetry *IEEE Trans. Geosci. Remote Sens.* **34** 498
[41] Cohen L 1989 Time-frequency distributions—a review *Proc. IEEE* **77** 941
[42] Collot G 1991 Fixed/rotary wings classification recognition *Proc. CIE 1991 Int. Conf. on Radar (CICR-91) (Beijing, China)* (Beijing: International Academic Publishers) p 610
[43] Cook C E and Bernfeld M 1967 *Radar Signals* (New York: Academic)
[44] Copeland J R 1960 Radar target classification by polarization properties *Proc. IRE* **48** 1290
[45] Daniels D J 1996 *Surface Penetrating Radar* (London: IEEE)
[46] Das Y and Boerner W-M 1978 On radar target shape estimation using algorithms for reconstruction from projections *IEEE Trans. Antennas Propag.* **26** 274
[47] DeGraaf S R 1998 SAR imaging via modern 2-d spectral estimation methods *IEEE Trans. Image Process.* **7** 729
[48] Delisle G Y and Wu H 1994 Moving target imaging and trajectory computation using ISAR *IEEE Trans. Aerosp. Electron. Syst.* **30** 887
[49] Dural G and Moffatt D L 1994 ISAR Imaging to identify basic scattering mechanisms *IEEE Trans. Antennas Propag.* **42** 99
[50] Feig E and Grünbaum A 1986 Tomographic methods in range-Doppler radar *Inverse Problems* **2** 185
[51] Felsen L B (ed) 1987 *Theoretical Aspects of Target Classification (AGARD Lecture Series No. 152)* (Munich: AGARD)
[52] Gerchberg R W 1979 Super-resolution through error energy reduction *Opt. Acta* **14** 709
[53] Gerry M J, Potter L C, Gupta I J and van der Merwe A 1999 A parametric model for synthetic aperture radar measurements *IEEE Trans. Antennas Propag.* **47** 1179
[54] Gross F B and Young J D 1981 Physical optics imaging with limited aperture data *IEEE Trans. Antennas Propag.* **29** 332
[55] Gupta I J 1994 High-resolution radar imaging using 2-D linear prediction *IEEE Trans. Antennas Propag.* **42** 31
[56] Harger R O 1970 *Synthetic Aperture Radar Systems* (New York: Academic)
[57] Hovenessian S A 1980 *Introduction to Synthesis Array and Imaging Radar* (Dedham, MA: Artech House Publishers)
[58] Hua Y, Baqai F and Zhu Y 1993 Imaging of point scatterers from step-frequency ISAR data *IEEE Trans. Aerosp. Electron. Syst.* **29** 195
[59] Huang C-C 1983 Simple formula for the RCS of a finite hollow circular cylinder *Electron. Lett.* **19** 854
[60] Hudson S and Psaltis D 1993 Correlation filters for aircraft identification from radar range profiles *IEEE Trans. Aerosp. Electron. Syst.* **29** 741
[61] Huynen J R 1978 Phenomenological theory of radar targets *Electromagnetic Scattering* ed P L E Uslenghi (New York: Academic) p 653
[62] Jain A and Patel I 1990 Simulations of ISAR image errors *IEEE Trans. Instrum. Meas.* **39** 212
[63] Johnson T W and Moffatt D L 1982 Electromagnetic scattering by open circular waveguides *Radio Sci.* **17** 1547
[64] Kachelmyer A L 1992 Inverse synthetic aperture radar image processing *Laser Radar* **7** 193
[65] Kalnins E G and Miller W Jr 1992 A note on group contractions and radar ambiguity functions *Institute for Mathematics and its Applications, Radar and Sonar* vol 39 (New York: Springer) p 71
[66] Keller J B 1959 The inverse scattering problem in geometrical optics and the design of reflectors *IRE Trans. Antennas Propag.* **7** 146
[67] Keller J B 1962 Geometrical theory of diffraction *J. Opt. Soc. Am.* **52** 116
[68] Kelly E J and Wishner R P 1965 Matched-filter theory for high-velocity, accelerating targets *IEEE Trans. Military Elec.* **9** 56
[69] Kennaugh E M 1952 Polarization properties of target reflection *Technical Report* 389–2 (Griffis AFB)
[70] Kennaugh E M and Moffatt D L 1965 Transient and impulse response approximations *IEEE Proc.* **53** 893
[71] Kennaugh E M 1981 The K-pulse concept *IEEE Trans. Antennas Propag.* **29** 327
[72] Kim H and Ling H 1993 Wavelet analysis of radar echo from finite-size targets *IEEE Trans. Antennas Propag.* **41** 200

[73] Kirk J C Jr 1975 Motion compensation for synthetic aperture radar *IEEE Trans. Aerosp. Electron. Syst.* **11** 338
[74] Kline M and Kay I W 1965 *Electromagnetic Theory and Geometrical Optics* (New York: Wiley)
[75] Knott E F and Senior T B A 1972 Cross polarization diagnostics *IEEE Trans. Antennas Propag.* **20** 223
[76] Kong K K and Edwards J A 1995 Polar format blurring in ISAR imaging *Electron. Lett.* **31** 1502
[77] Kouyoumjian R G and Pathak P H 1974 A uniform geometrical theory of diffraction for an edge in a perfectly conducting surface *Proc. IEEE* **62** 1448
[78] Kouyoumjian R G 1975 The geometrical theory of diffraction and its application *Numerical and Asymptotic Techniques in Electromagnetics* ed R Mittra (Berlin: Springer) p 165
[79] Ksienski D A 1985 Pole and residue extraction from measured data in the frequency domain using multiple data sets *Radio Sci.* **20** 13
[80] Langenberg K J, Brandfaß M, Mayer K, Kreutter T, Brüll A, Fellinger P and Huo D 1993 Principles of microwave imaging and inverse scattering *EARSeL Adv. Remote Sens.* **2** 163
[81] Lee S W and Deschamps G A 1976 A uniform asymptotic theory of EM diffraction by a curved wedge *IEEE Trans. Antennas Propag.* **24** 25
[82] Levanon N 1988 *Radar Principles* (New York: Wiley)
[83] Lewis R M 1969 Physical optics inverse diffraction *IEEE Trans. Antennas Propag.* **17** 308
Lewis R M 1970 *IEEE Trans. Antennas Propag.* **18** 194 (correction)
[84] Li H J and Yang S H 1993 Using range profiles as feature vectors to identify aerospace objects *IEEE Trans. Aerosp. Electron. Syst.* **41** 261
[85] Ling H, Chou R-C and Lee S W 1989 Shooting and bouncing rays: calculating the RCS of an arbitrary cavity *IEEE Trans. Antennas Propag.* **37** 194
[86] Madsen S N 1989 Estimating the Doppler centroid of SAR data *IEEE Trans. Aerosp. Electron. Syst.* **25** 134
[87] Mager R D and Bleistein N 1978 An examination of the limited aperture problem of physical optics inverse scattering *IEEE Trans. Antennas Propag.* **26** 695
[88] Maitre H 1981 Iterative superresolution: some new fast methods *Opt. Acta* **28** 973
[89] Mandel L 1974 Interpretation of instantaneous frequency *Am. J. Phys.* **42** 840
[90] Marin L and Latham R W 1972 Representation of transient scattered fields in terms of free oscillations of bodies *IEEE Proc.* **60** 640
[91] Marin L 1973 Natural-mode representation of transient scattered fields *IEEE Trans. Antennas Propag.* **21** 809
[92] Mensa D, Heidbreder G and Wade G 1980 Aperture synthesis by object rotation in coherent imaging *IEEE Trans. Nucl. Sci.* **27** 989
[93] Mensa D L 1981 *High Resolution Radar Imaging* (Dedham, MA: Artech House Publishers)
[94] Mensa D L, Halevy S and Wade G 1983 Coherent Doppler tomography for microwave imaging *Proc. IEEE* **71** 254
[95] Merserau R M and Oppenheim A V 1974 Digital reconstruction of multidimensional signals from their projections *Proc. IEEE* **62** 1319
[96] Mevel J 1976 Procedure de reconnaissance des formes l'ide d'un radar monostatique *Ann. Telecommun.* **131** 111
[97] Moffatt D L and Mains R K 1975 Detection and discrimination of radar targets *IEEE Trans. Antennas Propag.* **23** 358
[98] Moghaddar A and Walton E K 1993 Time-frequency distribution analysis of scattering from waveguides *IEEE Trans. Antennas Propag.* **41** 677
[99] Mohammad-Djafari A and Demoment G 1989 Maximum entropy Fourier synthesis with application to diffraction tomography *Appl. Opt.* **26** 1745
[100] Moll J W and Seecamp R G 1969 Calculation of radar reflecting properties of jet engine intakes using a waveguide model *IEEE Trans. Aerosp. Electron. Syst.* **6** 675
[101] Molyneux J E 1995 Ground penetrating radar tomography *Int. Conf. Acoust. Speech and Signal Proc. Conf. Proc.* vol 5 (New York: IEEE) p 2813
[102] Moore J and Ling H 1995 Super-resolved time-frequency analysis of wideband backscattered data *IEEE Trans. Antennas Propag.* **43** 623
[103] Moran B 2000 Mathematics of radar signal processing *Twentieth Century Harmonic Analysis—A Celebration (NATO Science Series II: Mathematics and Chemistry, vol 33)* ed J S Byrnes (Dordrecht: Kluwer Academic) ch 14
[104] Morgan M A 1984 Singularity expansion representations of fields and currents in transient scattering *IEEE Trans. Antennas Propag.* **32** 466
[105] Morgan M A 1988 Scatterer discrimination based upon natural resonance annihilation *J. Electromagn. Waves Appl.* **2** 481
[106] Müller C 1969 *Foundations of the Mathematical Theory of Electromagnetic Waves* (New York: Springer)

[107] Munson D C, O'Brien D and Jenkins W K 1983 A tomographic formulation of spotlight-mode synthetic aperture radar *Proc. IEEE* **71** 917
[108] Noel B (ed) 1991 *Ultra-Wideband Radar Proc. First Los Alamos Symp.* (New York: CRC Press)
[109] North D O 1943 An analysis of the factors which determine signal-noise discrimination in pulsed carrier systems *RCA Lab. Report* PTR-6C
[110] Nuttall A H 1966 On the quadrature approximation to the Hilbert transform of modulated signals *IEEE Proc.* **54** 1458
[111] Odendaal J W, Barnard E and Pistorius C W I 1994 Two-dimensional superresolution using the MUSIC algorithm *IEEE Trans. Aerosp. Electron. Syst.* **42** 1386
[112] Pathak P H, Chuang C W and Liang M C 1986 Inlet modeling studies *Ohio State University, ElectroScience Lab Report* 717674-1 *(Oct. 1986)*
[113] Pathak P H and Burkholder R J 1991 High-frequency electromagnetic scattering by open-ended waveguide cavities *Radio Sci.* **26** 211
[114] Pearson L W 1983 Present thinking on the use of the singularity expansion in electromagnetic scattering computation *Wave Motion* **5** 355
[115] Pham D T 1998 Applications of unsupervised clustering algorithms to aircraft identification using high range resolution radar *Non-Cooperative Air Target Identification Using Radar (AGARD Symp. RTO-MP-6) (Mannheim, Germany, April)* (Quebec: Canada Communications Group) paper 16
[116] Poggio A J and Miller E K 1973 Integral equation solutions to three-dimensional scattering problems *Computer Techniques for Electromagnetics* ed R Mittra (London: Pergamon)
[117] Potter L C, Chiang D, Carriere R and Gerry M J 1995 A GTD-based parametric model for radar scattering *IEEE Trans. Antennas Propag.* **43** 1058
[118] Potter L C and Moses R L 1997 Attributed scattering centers for SAR ATR *IEEE Trans. Image Process.* **6** 79
[119] Prickett M J and Chen C C 1980 Principles of inverse synthetic aperture radar (ISAR) imaging *IEEE 1980 EASCON Record* 340
[120] Raney R K 1971 Synthetic aperture radar and moving targets *IEEE Trans. Aerosp. Electron. Syst.* **7** 499
[121] Rhebergen J B, van den Berg P M and Habashy T M 1997 Iterative reconstruction of images from incomplete spectral data *Inverse Problems* **13** 829
[122] Rihaczek A W and Hershkowitz S J 1996 *Radar Resolution and Complex-Image Analysis* (Dedham, MA: Artech House Publishers)
[123] Rihaczek A W and Hershkowitz S J 1996 Man-made target backscattering behavior: applicability of conventional radar resolution theory *IEEE Trans. Aerosp. Electron. Syst.* **32** 809
[124] Rihaczek A W 1969 *Principles of High-Resolution Radar* (New York: McGraw-Hill)
[125] Rosenbaum-Raz S 1967 On scatterer reconstruction from far-field data *IEEE Trans. Antennas Propag.* **24** 66
[126] Ross D C, Volakis J L and Hristos T A 1995 Hybrid finite element analysis of jet engine inlet scattering *IEEE Trans. Antennas Propag.* **43** 277
[127] Skolnik M L 1980 *Introduction to Radar Systems* 2nd edn (New York: McGraw-Hill)
[128] Smith C R and Goggans P M 1993 Radar target identification *IEEE Antennas Propag. Mag* **35** 27
[129] Sparr T, Hamran S and Korsbakken E 2000 Estimation and correction of complex target motion effects in inverse synthetic aperture imaging of aircraft *Record of the IEEE 2000 Int. Radar Conf.* p 457
[130] Stark H (ed) 1987 *Image Recovery: Theory and Practice* (Orlando, FL: Academic)
[131] Steinberg B D 1988 Microwave imaging of aircraft *IEEE Proc.* **76** 1578
[132] Stratton J A 1941 *Electromagnetic Theory* (New York: McGraw-Hill)
[133] Stuff M A, Sullivan R C, Thelen B J and Werness S A S 1994 Automated two and three-dimensional, fine resolution, radar imaging of rigid targets with arbitrary unknown motion *(SPIE Proc.)* vol 2230 p 180
[134] Sullivan R J 2000 *Microwave Radar Imaging and Advanced Concepts* (Boston, MA: Artech House Publishers)
[135] Swick D A 1969 A review of wideband ambiguity functions *NRL Report* 6994
[136] Tabbara W 1973 On an inverse scattering method *IEEE Trans. Antennas Propag.* **21** 245
[137] Tabbara W 1975 On the feasibility of an inverse scattering method *IEEE Trans. Antennas Propag.* **23** 446
Tabbara W 1977 *IEEE Trans. Antennas Propag.* **25** 286 (correction)
[138] Trintinalia L C and Ling H 1996 Extraction of waveguide scattering features using joint time-frequency ISAR *IEEE Microw. Guid. Wave Lett.* **6** 10
[139] Trintinalia L C and Ling H 1997 Joint time-frequency ISAR using adaptive processing *IEEE Trans. Antennas Propag.* **45** 221
[140] Trischman J, Jones S, Bloomfield R, Nelson E and Dinger R 1994 An X-band linear frequency modulated radar for dynamic aircraft measurement *AMTA Proc. (Long Beach, CA)* (Atlanta, GA: AMTA) p 431
[141] Trischman J A 1996 Real-time motion compensation algorithms for ISAR imaging of aircraft *SPIE Proc. Radar/Ladar Proc. and Appl. (Denver, CO)* (Bellingham, WA: SPIE) p 110

[142] Tsao J and Steinberg B D 1988 Reduction of sidelobe and speckle artifacts in microwave imaging: the CLEAN technique *IEEE Trans. Antennas Propag.* **36** 543
[143] Ueberschaer R 1992 Double-scatter tracks in 1D and 2D images *IEEE Antennas Propag. Soc Int. Symp.* vol 3 p 1714
[144] Ufimtsev P 1962 The method of fringe waves in the physical theory of diffraction *Sovyetskoye Radio* (Moscow)
[145] VanBlaricum M L and Mittra R 1975 A technique for extracting the poles and residues of a system directly from its transient response *IEEE Trans. Antennas Propag.* **23** 777
[146] Wahl D E, Eichel P H, Ghiglia D C and Jakowatz C V Jr 1994 Phase gradient autofocus—a robust tool for high resolution SAR phase correction *IEEE Trans. Aerosp. Electron. Syst.* **30** 827
[147] Walker J L 1980 Range-Doppler imaging of rotating objects *IEEE Trans. Aerospace Electron. Syst.* **16** 23
[148] Wang T M and Ling H 1991 Electromagnetic scattering from three-dimensional cavities via a connection scheme *IEEE Trans. Antennas Propag.* **39** 1501
[149] Wang Y, Ling H and Chen V C 1998 ISAR motion compensation via adaptive joint time-frequency technique *IEEE Trans. Aerosp. Electron. Syst.* **34** 670
[150] Wang Y M and Chew W C 1993 A recursive T-matrix approach for the solution of electromagnetic scattering by many spheres *IEEE Trans. Antennas Propag.* **41** 1633
[151] Watanabe Y, Itoh T and Sueda H 1996 Motion compensation for ISAR via centroid tracking *IEEE Trans. Aerosp. Electron. Syst.* **32** 1191
[152] Wehner D R 1987 *High Resolution Radar* (Norwood, MA: Artech House Publishers)
[153] Wehner D R, Prickett M J, Rock R G and Chen C C 1979 Stepped frequency radar target imagery, theoretical concept and preliminary results *Technical Report* 490, Naval Ocean Systems Command, San Diego, CA
[154] Weiss M R 1968 Inverse scattering in the geometric-optics limit *J. Opt. Soc. Am.* **58** 1524
[155] Werness S, Carrara W, Joyce L S and Franczak D B 1990 Moving target imaging algorithm for SAR data *IEEE Trans. Aerosp. Electron. Syst.* **26** 57
[156] Witt H R and Price E L 1968 Scattering from hollow conducting cylinders *Proc. IEE* **115** 94
[157] Woodward P M 1953 *Probability and Information Theory with Applications to Radar* (New York: Pergamon)
[158] Wu H, Grenier D and Fang D 1995 Translational motion compensation in ISAR processing *IEEE Trans. Image Process.* **4** 1561
[159] Wu H and Delisle G Y 1996 Precision tracking algorithms for ISAR imaging *IEEE Trans. Aerosp. Electron. Syst.* **32** 243
[160] Xu X and Narayanan R M 2001 Three-dimensional interferometric ISAR imaging for target scattering diagnosis and modeling *IEEE Trans. Image Process.* **10** 1094
[161] Zyweck A and Bogner R E 1996 Radar target classification of commercial aircraft *IEEE Trans. Aerosp. Electron. Syst.* **32** 598